Research of influence of different shaped charge liner materials on penetration depth using numerical simulations

Alan Catovic[1]

[1] Defense Technology Department, Mechanical Engineering Faculty, University of Sarajevo, Bosnia

ABSTRACT

Numerical simulations, using the Ansys AUTODYN program, of Panzerfaust 30 (klein) anti-tank warhead, were performed to determine the influence of different liner materials on the penetration depth into a steel target. It has been shown that the choice of liner material can significantly affect the performance of the ammunition. Along with other methods of optimizing shaped charge ammunition (optimization of the shape, thickness and angle of the tip of the liner, use of more potent explosive and deviator, optimization of casing thickness and stand-off distance, etc.), the use of appropriate liner material is certainly one of the most important parameters of shaped charge warheads to consider. Together with analytical calculations and experimental tests, simulations are a valuable tool. Using data obtained from numerical simulations, researchers can save both time and resources during the process of munition design and optimization.

Keywords:　　　　　shaped charge, HEAT warhead, Panzerfaust 30, liner material, penetration depth

Corresponding Author:

Alan Catovic
Defense Technology Department
University of Sarajevo
Vilsonovo setaliste 9, Sarajevo, Bosnia
E-mail: catovic@mef.unsa.ba

1. Introduction

HEAT (High Explosive Anti Tank) warheads, thanks to their construction characteristics, represent a specific design of HE warheads. A shaped charge explosion is oriented in space in the pre-selected direction. After the initiation of the explosive charge, the propagation of the detonation wave begins through the explosive at the detonation velocity of the given explosive. When the front of the detonation wave hits the liner, the material of the liner is subjected to very high pressure (10-40 GPa) and begins to collapse towards the axis of symmetry of the liner, colliding with it. This collision, primarily due to the high pressure, results in the movement of the liner material along the axis of symmetry into a high-speed jet (up to 12 km/s) and slug (up to 3 km/s) [1,7,8,11].

To estimate the penetration depth of HEAT ammunition, the following methods are generally used: [2,3]:

- Analytical methods (models of Birkhoff, Eichelberger, Hill, Evans, Mott, Pack, Pugh, Allison, Dipersio, Simon, Merendino, etc.), with frequently using programs (such as BASC, DESC, TEMPS, PISCES 2DELK),
- experimental tests (mostly on RHA/Rolled Homogeneous Armour target), and
- numerical simulations (for example Ansys LS DYNA and AUTODYN, ABAQUS, CTH, HEMP, EPIC, WAVE, HULL).

In this paper, the focus will be on numerical simulations since they can significantly reduce time in the design process.

Mass, momentum, and energy conservation equations are used in continuum mechanics formulations along with a corresponding description of material behavior to perform numerical simulations of phenomena such as

the interaction of explosives and metals or penetration at extremely high velocities. Defining the initial and boundary conditions pertinent to the given situation completes the formulations. The result is a nonlinear system of partial differential equations. Problems solved by numerical simulations include highly dynamic loads produced by impact or detonation in a very short amount of time. For simulating the collapse of a shaped charge liner, the detonation gases' behavior is first considered before the energy imparted to the liner materials is calculated. Computer programs that are designed for numerical simulations of the non-stationary problems of continuum mechanics are known in the literature as continuum mechanics codes, wave propagation codes, hydrodynamic codes, or hydrocodes (the name arose because in early computer models, the strength of the material was not considered due to the high velocity and pressure of the process) [4].

Generally, the parameters that influence the penetration depth of HEAT ammunition are warhead caliber, type of material (liner, explosive chain (detonator, booster, main charge), casing, and target), standoff (distance between the bottom of the liner and the target), geometric parameters of the liner (shape, thickness, angle of liner apex), rotation of the projectile, deviator parameters (shape, mass, material, position), fuze type, etc. The performance of HEAT warhead depends also on the manufacturing methods (concentricity of components, explosive charge homogeneity, etc).

The purpose of the research is to study the effects of different liner materials of HEAT warhead on its penetration depth using numerical simulations. Using data obtained from numerical simulations, researchers can save both time and resources during the process of munition design and optimization. Together with analytical calculations, and experimental tests, numerical simulation can be a valuable design tool.

2. Review of literature

Walters and Zukes in their seminal book [1] describe important aspects of shaped charges (jet formation, the breakup of jets, penetration models, influencing parameters, computational aspects, and wave propagation codes), including history and applications. They emphasize that liner material is of paramount importance. Liner material may even consist of two (or more) materials (for example stratified, layered bimetallic liners). Favorable characteristics of shaped charge liner materials include high melting point, high density, high sound speed (to guarantee jet cohesiveness), high dynamic strength (under high strain-rate conditions), fine grain with proper orientation (results in high yield stress with good elongation and higher hardness; yield stress and material hardness are increased when the grain size decreases), nontoxicity, as well as availability, low expenses, and ease of production (these requirements preclude platinum or gold (expensive), osmium (not readily available), etc). High ductility, jet coherency, advantageous velocity gradient, more massive jet, high velocity of jet, and jet with extended break-up time are all features of suitable shaped charge jets. The "factor of merit (FoM)," $FoM = V_j \tau \sqrt{\rho_p} / CD$, where V_j is the jet tip velocity, τ is the jet average breakup time, ρ_j is the jet density, and CD is the charge diameter, can be used to evaluate the performance of shaped charges.

Zukas [2] gives an introduction to impact phenomena, material characterization and failure at high-strain rates, and analytical models for penetration. He also gives a review of experimental methods for terminal ballistics and impact physics, as well as a review of computer codes for impact simulation.

Carleone [3] describes warhead simulation techniques with hydrocodes and gives a review of the mechanics of shaped charges and penetration models.

Zukas [4] describes the dynamic behavior of materials and structures, wave propagation, impact and shock waves in solids, gives an introduction to numerical modeling of fast, transient phenomena, and describes lucidly how a hydrocode really works. He also describes some of the experimental methods for material behavior at high strain rates.

Gurel [5] in his thesis describes the modeling of shaped charge using analytical and numerical methods. He performed numerical simulations (using Lagrange and Euler solver) of jet formation and penetration with Ansys AUTODYN.

Fišerová [6] describes an approach (using AUTODYN program) for numerical modeling of soil-blast interaction in landmine explosions with lucid and useful explanations.

Poole [7] developed a mathematical model for the jet penetration into a solid target, where the model couples fluid dynamics in the jet with elastic-plastic solid mechanics in the target.

Held [8] evaluated the properties of individual liner materials. He noticed that besides proven material such as copper - tungsten, tantalum, nickel, depleted uranium and molybdenum also have potentially good properties for shaped charges. Shaped charge penetration potential is directly proportional to the square root of the density of the liner material and maximum jet length. The bulk sound velocity of the liner material influences the jet-tip velocity. The ductility of the liner material, which is primarily determined by the material crystal structure, strongly influences the particulation time (breakup time) of the jet. The jet elongates up to 1000% or 2000% compared to the original length of the liner (for copper), with a strain rate 10^4 - 10^3 s^{-1}, before it breaks up into the discrete jet particles (because of the velocity gradient between the jet tip and the slug). The greatest attainable jet tip velocity, as a general rule, is 2.34 times the bulk sound velocity of the liner material. Longer jet particulation times are produced by the fine crystal structures, increasing the jet length. The crystal structure of the liner material depends on the crystal structure of the raw materials and the liner's manufacturing methods.

Wang et al [9] describe the influence of liner material (Cu, Al, steel) on jet formation and penetration capability, using tests and numerical simulations. They concluded that the copper jet, with a velocity somewhat greater than the steel jet but lower than the aluminum jet, has the highest penetrating capability (for the materials chosen). Aluminum jet has the highest velocity but the lowest penetration capability (lower density).

Elshenawy [10] in his thesis provided a thorough review of shaped charge phenomenology, including factors affecting the shaped charge, jet formation, and penetration models, and hydrocode simulations (with parametric analysis).

Kulsirikasem et al [11] investigated materials for liners of shaped charge warheads and optimum standoff distances, using numerical simulations. Euler mesh was used to model the air, explosive, liner, and target while the casing was modeled with Lagrange mesh. They used jet momentum as the main parameter indicating jet penetration capability since the penetration capability mainly depends on the density and velocity of the jet.

The resources of the raw materials for shaped charge liners, their qualities, and their costs are summarized by Buc [12]. Copper (OFHC version is the optimal choice) is the most frequently used material for shaped charge liners and EFP. Tested alloys include Cu/Ni, Cu/Ag, and others. The density of copper is 8,9 g/cm^3, the melting temperature 1083 °C, and sound speed 4,7 km/s. Copper provides excellent jet ductility. Aluminum was used in AGM-65 Maverick warhead, as well as an experimental precursor for high-speed jet applications and enhanced blast warheads (exothermally reactive). The density of aluminum is 2,7 g/cm^3, the melting point is 675 °C, and the sound speed is 6,4 km/s. It has good jet ductility and it is pyrophoric. Gold has a high density (beneficial) of 19,3 g/cm^3 but a low sound speed (not beneficial) of 3,2 km/s, so it may be no better than uranium liners. The melting point of gold is 1064 °C and gold has excellent corrosive resistance in the air. The advantage of gold may be its ductility, if it leads to greatly improved jet breakup parameters, compared to its cost. Molybdenum shaped charge liners are used for high-speed jet applications. The density of molybdenum is 10,2 g/cm^3, the melting point is very high (2610 °C), and sound speed is 6,4 km/s. Silver may have potential if its ductility translates into better breakup times for jets. The density of silver is 10,5 g/cm^3, the melting point is 961 °C, and sound speed is 3,6 km/s. Tantalum is candidate liner for missiles and torpedos, as well as liner for SADARM submunition. The density of tantalum is 16,6 g/cm^3, the melting point is high (2996 °C), and sound speed is 4-4,5 km/s. It has good jet ductility. Tungsten is also attractive because of high density (19,25 g/cm^3) and high sound speed (5,2 km/s). Tungsten also shows good ductility during shaped charge jetting, even though it is very brittle at ambient conditions. Uranium can also be used as EFP liner (ie. alloyed with niobium), with a density of 19,05 g/cm^3, the sound speed of 2,5-3 km/s, and the melting point of 1133 °C. It is highly pyrophoric which is favorable characteristic. Zirconium can be used as a shaped charge liner for enhanced behind armor effects (pyrophoric effect). The density of zirconium is 6,49 g/cm^3, the melting point is high (1852 °C), and sound speed is 4,62 km/s [12].

Johnson and Cook [13] presented a constitutive model and data for following materials subjected to large strains, high strain rates and high temperatures: OFHC copper, cartridge brass, Nickel 200, Armco iron, Carpenter electrical iron, 1006 steel, 2024-T351 aluminum, 7039 aluminum, 4340 steel, S-7 tool steel, Tungsten alloy and DU-.75Ti (depleted uranium). Torsion tests at various strain rates, static tensile tests, dynamic Hopkinson bar tensile tests, and Hopkinson bar tests at high temperatures are used to gather the data for these material constants.

Generally, the most commonly used liner material is copper, which has a surface-centered cubic crystal structure, suitable for achieving good ductility. Molybdenum (a volume-centered cubic crystal structure, which is inherently less ductile) is also widely used as a liner material. In general, metals with a volume-centered cubic structure (Fe, Mo, Ta) tend to produce thicker jets, while metals with a surface-centered cubic lattice produce long thin ductile jets. Materials with a hexagonal crystal lattice (Mg, Ti) tend to produce powdered jets (in such structures, less plastic deformation occurs under impulse loading).

Researchers from Ballistic Research Laboratory tested various materials for potential liner application. They noticed that good, ductile (property of a material to withstand plastic deformation without breaking) jets are given by: aluminum, copper, gold, lead, nickel, platinum, silver and tungsten. Lower ductility jets are provided by: chromium, iron, lithium, molybdenum, tantalum and vanadium. Intermittent ("powder") jets are given by: beryllium, boron, cadmium, carbon, cobalt, magnesium, osmium, titanium, zinc and zirconium. They also tested various alloys: multiphase (95Cu-5Al, 90Cu-10Sn, 90Cu-10Zn, 70Cu-30Zn, 304SS, IN-744), solid solutions (90Cu-10Ni, 70Cu-30Ni, 50Cu-50Ni, 30Cu- 70Ni), eutectic (38Pb-62Sn, 89Pb-11Sb, 28Cu-72Ag), eutectoid (78Zn-22Al) and pressed/sintered variants (90W-7Ni-3Fe, 78W-22Cu, 70W-30Cu). They concluded the following. Liners from Be can produce high velocities but low jet masses. Mg and Zr show combustible effects. Depleted uranium, with appropriate design and thermal treatment, gives a jet of excellent quality. Cu-Y alloy with conical liner geometry gives a continuous jet of fine particles, and in the hemispherical shape of the liner, the jet was very ductile with a long breakup time. Liners made of an alloy of depleted uranium and nickel in a hemispherical shape give a continuous jet that does not break. Multiphase liners proved to be the worst option (incoherent jet and early jet fragmentation). Solid solution alloy liners can form coherent jets but are not ductile. Eutectic alloys usually give continuous jets, without breakup. They show excellent penetration into steel targets. Eutectoid alloys did not show good properties for the jet. Their jets are interrupted and spread out radially. Pressed/sintered liners give a continuous jet of fine particles, but the jets tend to disperse over larger standoff distances and vary in quality. They also mention diffusion-bonded alternately layered liners (for example layered copper-nickel hemispherical liner) [14].

Ding et al [15] in their research (estimation of parameters for tandem shaped charge) considered the influence of the type of liner material on the value of jet velocity. They concluded, based on numerical simulations, that liners made of amorphous material - acrylic glass (lucite, plexiglass) potentially have excellent ductility and form a jet of great length and speed. At the same time, such liners have a smaller mass than copper ones, which can be useful, for example, in the design of tandem-shaped charges.

Fu and Rong [16] used alloys of Cu and tungsten for the liner and the experiments were done using flash x-ray. Improved penetration was observed due to the increased material density and breakup time.

Bourne et al [17] used silver, titanium, zirconium, and depleted uranium (DU) as hemispherical liners. These materials provided ductile jets with longer breakup times than copper, due to the intrinsic material properties of these metals. This implies that compared with copper, these materials can potentially provide better penetration performance. The use of DU for the liner is generally considered not practical due to its toxicity (and radiation) hazards.

Copper-tungsten alloys used as material for shaped charge liners [18] lead to an increase in the jet penetration depth into a steel target (an increase of 30% in comparison with copper jets). The improvement is due to the increase of both the density and the breakup time. The addition of zinc and nickel in the Cu-W alloy decreases target penetration because of the radial dissipation of jet energy [19].

Increased magnetic field reduces penetration of jets (the magnetic field was produced in a shaped-charge liner before firing), as evidenced by the effect it has on a Cu liner [20].

Cu, carbon steel, and Ti-6Al-4V alloy were chosen [21] as the three target materials for Cu-W shaped charge jet penetration. The ratio of penetration depths were discovered to be 10:28:21, which showed that the same jet behaved differently depending on the target material.

Numerical simulations and experiments [22] showed that the conical Al liner has higher destructive power than Cu liners in concrete targets. Considering costs, Cu and Al are the best choices for RHA and concrete-like targets respectively.

Xiao et al [24] performed experiments to investigate the enhanced lethality of reactive materials (mixture of Al and PTFE) shaped charge liners against a concrete target.

The main methods for producing metallic liners are, generally, rolling, die-pressing, and machining. To make the liners from metal powder through sintering, researchers turned to powder metallurgy. It involves pressing or heating granules into a solid state without melting them. A review of metallurgical advancements for powder liners can be found in [23]. Zygmunt conducted experiments with powder liners (Cu and Cu-W) [25], showing that powder metallurgy technology allows for the design and production of liners in a variety of geometries and chemical compositions, as well as small calibers up to several dozen millimeters. The performance of shaped charges made with powder liners (43% copper, 45% tungsten, 11% tin, 1% graphite) was investigated in a study by Walters et al [26]. Flash radiography was used to determine jet characteristics as a penetrator as well as its penetration depth and hole size through (RHA) plate at various standoff distances. An excessive round-to-round variability in the penetration was observed, especially at longer standoffs. Theoretical considerations on the penetration of powdered metal jets can be found in [27].

Duan et al [28] used sintered and non-sintered Cu liners with particle sizes below 20 μm. Research revealed that the sintered Cu powder liner is denser, has a thinner wall, and has better penetration than the non-sintered one.

The reactivity of liners can be increased by adding Al to Cu liners, with reactive liners having larger holes but smaller penetration depth [29].

Copper powder coated with graphene was also used as potentially shaped charge liner material [30]. Isostatic pressing allows for the creation of sinters with densities that are over 8% greater than those of die-pressed materials. The latter, though, is better suited for mass production.

Santosh et al [31] concluded that bimetallic shaped charge liner shows better penetration depths (15,8% increase shown in tests) than monolithic liner. The liner of the outer cone (aluminum; in contact with explosive) mostly goes in the slug, with a large portion of it vaporizing, while liner of the inner cone (copper) mostly constitutes the jet.

Regarding the target material influence on shaped charge total penetration depth, Elshenawy et al [36] found penetration depth to decrease in average about 0,07 mm per 1 MPa increase in the yield strength of the target material, which was validated over a wide range of target yield strength (0,47 GPa to 1,8 GPa). They also provided empirical relation between cut-off velocity (defined as a velocity of the last penetrating element of jet [10] or minimum jet velocity for penetration) and the relevant target yield strength. For steel with yield strength of 1 GPa, cut-off velocity was found to be around 1400 m/s; for yield strength of 0,47 GPa, cut-off velocity was around 1150 m/s; the largest cut-off velocity reported was 1820 m/s for yield strength of 1,8 GPa.

El-Sayed et al [37] varied different parameters (liner thickness, material, and apex angle, type of explosive and standoff distance) of the shaped charge. By selecting optimal parameters (optimal liner thickness, shape, materials, and standoff distance) they were able to significantly increase penetration depth (up to around 30%).

In a constant liner mass hemispherical warhead design, Bourne et al. [55] examined the performance of liners made of depleted uranium (DU), copper, titanium, silver, and zirconium. Zirconium was shown to have the longest breakup time, greatest cumulative jet length, and fastest tip velocity. Also, it is clear that all of the metals tested had slower break-up times than copper. The silver, zirconium, and DU jet's low plastic particle velocity suggests that these materials are more ductile than copper. Yet since the DU is toxic, it cannot be used as a shaped charge liner.

The performance of liners made from a combination of electrolytic copper and tungsten was studied by Zygmunt and Wilk [56]. The resulting (ECu/W) liner, which was created using a powder metallurgical process and was made from a mixture of copper and tungsten powder, showed a lower jet tip velocity but deeper penetration than standard copper liner because of a higher density (12.5 g/cm^3).

Fuchs [63] described the use of porous tungsten as a liner for shaped charges to improve their penetration depth. In his research he presented different materials (adapted from [64]) having a higher density than copper, which would be potentially more effective than copper as a liner material for shaped charges (table 2.1). A selection of materials that could be utilized to create improved shaped charges is formed by choosing those from this list in table 2.1 that has a higher density and a higher speed of sound than copper. These materials are molybdenum, rhodium, rhenium, tungsten, and palladium, listed from highest to lowest sound

speed. These sound speeds are obtained using shock speed/particle velocity measurements, and they are based on high-pressure shock conditions. They differ from the conventionally determined and reported speeds of elastic sound in literature.

Table 2.1 Material properties from selected Hugoniots [63,64]

Material	Density (g/cm^3)	Speed of sound (km/s)
Iridium	22.284	3.916
Platinum	21.419	3.598
Rhenium	21.021	4.184
Gold	19.240	3.056
Tungsten	19.224	4.029
Tantalum	16.654	3.414
Mercury	13.540	1.490
Hafnium	12.885	2.964
Rhodium	12.428	4.807
Palladium	11.991	3.948
Thallium	11.840	1.862
Thorium	11.680	2.133
Lead	11.350	2.051
Silver	10.490	3.229
Molybdenum	10.206	5.124
Bismuth	9.836	1.826
Copper	8.930	3.940

3. Overview of Panzerfaust 30 (klein) HEAT munition

Research of the influence of different shaped charge liner materials on penetration depth using numerical simulations was performed on Panzerfaust 30 (klein) HEAT warhead which certainly had historical importance**.** This system was interesting and one of the first shaped charge anti-tank weapons used. The first Panzerfaust (germ. Tank devil) anti-tank system (Panzerfaust 30) was developed in HASAG (Hugo Schneider Action Gesellschaft, Leipzig) to fight primarily against the increasing numbers and quality of Russian tanks. The Panzerfaust system (Figure 3.1) was designed to give the soldier personal anti-tank protection. The Panzerfaust 60 replaced the Panzerfaust 30 during the summer of 1944 but development continued and soon after, the Panzerfaust 100 appeared. Numbers behind the name indicate the effective range achievable (horizontal dispersion was larger than vertical [40]). A total of around 8-9 million Panzerfaust systems were manufactured during II World war [38,39,44], with significant impact during the war (in comparison, the US produced 15,6 million Bazookas [40]).

The Panzerfaust 30 (klein) HEAT warhead had a mass of 1,3 kg (total mass of 3,2 kg), with a warhead diameter of 95 mm, a launch tube diameter of 33 mm, an initial velocity of 28 m/s, and a penetration depth of 140 mm through armour steel. The depth of penetration was 1270 mm through sandbags and 250 mm through reinforced concrete; these tests were conducted since allied tanks were provided with sandbags and concrete plates over base steel armor as additional protection (Panzerfaust was more effective than Bazooka regarding sandbags and concrete, so it was frequently used against mentioned targets) [38,39,40,44]. While additional sandbags on tanks could decrease the depth of penetration achieved by the Panzerfaust warhead, there was enough residual energy left to penetrate the glacis plate of the M4 medium tank. US Army Ordnance officers felt that shaped charge warheads needed at least 51 mm of penetrating power beyond the energy needed to penetrate the armor plate to cause significant damage within the tank. To be effective against a tank such as the M4 with its 90 mm (equivalent) frontal armor required a warhead with 140 mm penetrating power (90+50 mm) to have lethal internal effects which was within the capability of the Panzerfaust 30 (klein) [39].

The main charge in the Panzerfaust warhead was RDX/TNT mixture (Composition B), with PETN/Wax mixture as a booster charge [38,42,43,50]. It is not known how was the warhead filled with explosive (pressing or casting). Also, some authors mention Pentol (PETN/TNT) as a main explosive charge [40], but substituting PETN for RDX leads to a decrease in the efficiency of shaped charges [42]. The propellant, with a mass of 53.5 g, used in Panzerfaust was GP - powdered sodium picrate combined with a binding agent such as Igetex (copolymer of butadiene and styrene) [40,42].

Panzerfaust 30 (klein)

1. Shaped-charge cavity (*Hohlladung*) and liner (*Einlage*)
2. high-explosive filler
3. Locking collar
4. Booster charge (kleine Zündladung 34)
5. Faustpatronezünder FPZ 8001
6. Tail shaft with four folding tailfins (one shown)
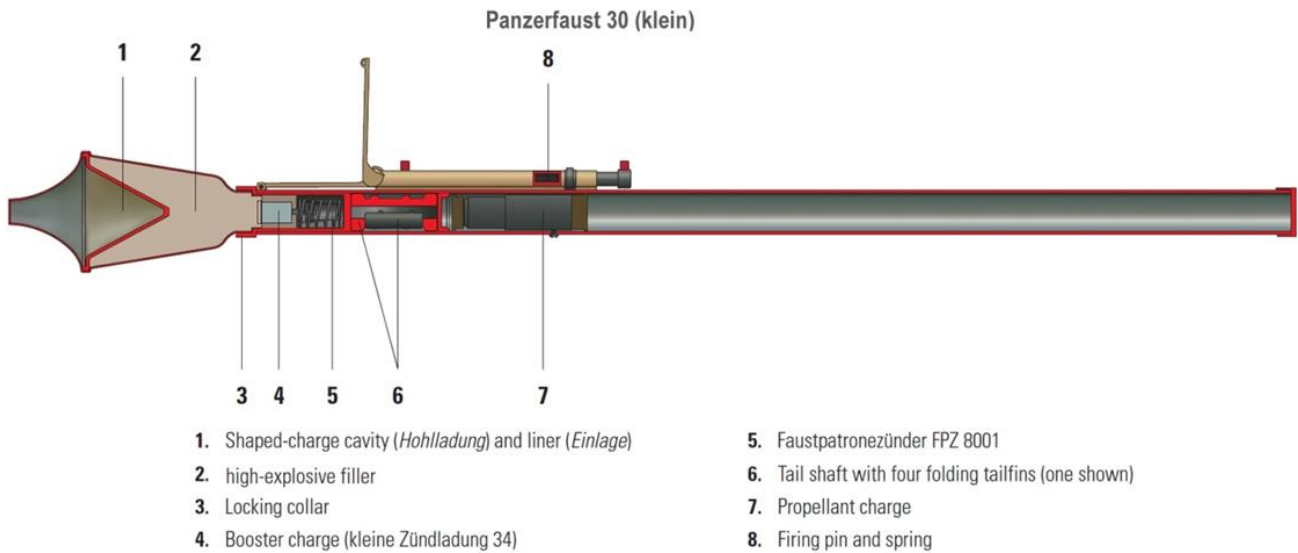7. Propellant charge
8. Firing pin and spring

Figure 3.1 Panzerfaust 30 (klein) munition and launcher cross-section [adapted from 40]

Data on the thicknesses of the shaped charge liner and casing, made both of sheet steel [40] (copper was in short supply), of the Panzerfaust warhead were not available so from available drawings [41] it was deduced, using CAD methods and scaling (Figure 3.2), that the thicknesses of the liner and casing were 3 mm and 1 mm, respectively. Using the same method it was concluded the liner had apex half-angle of 28°.
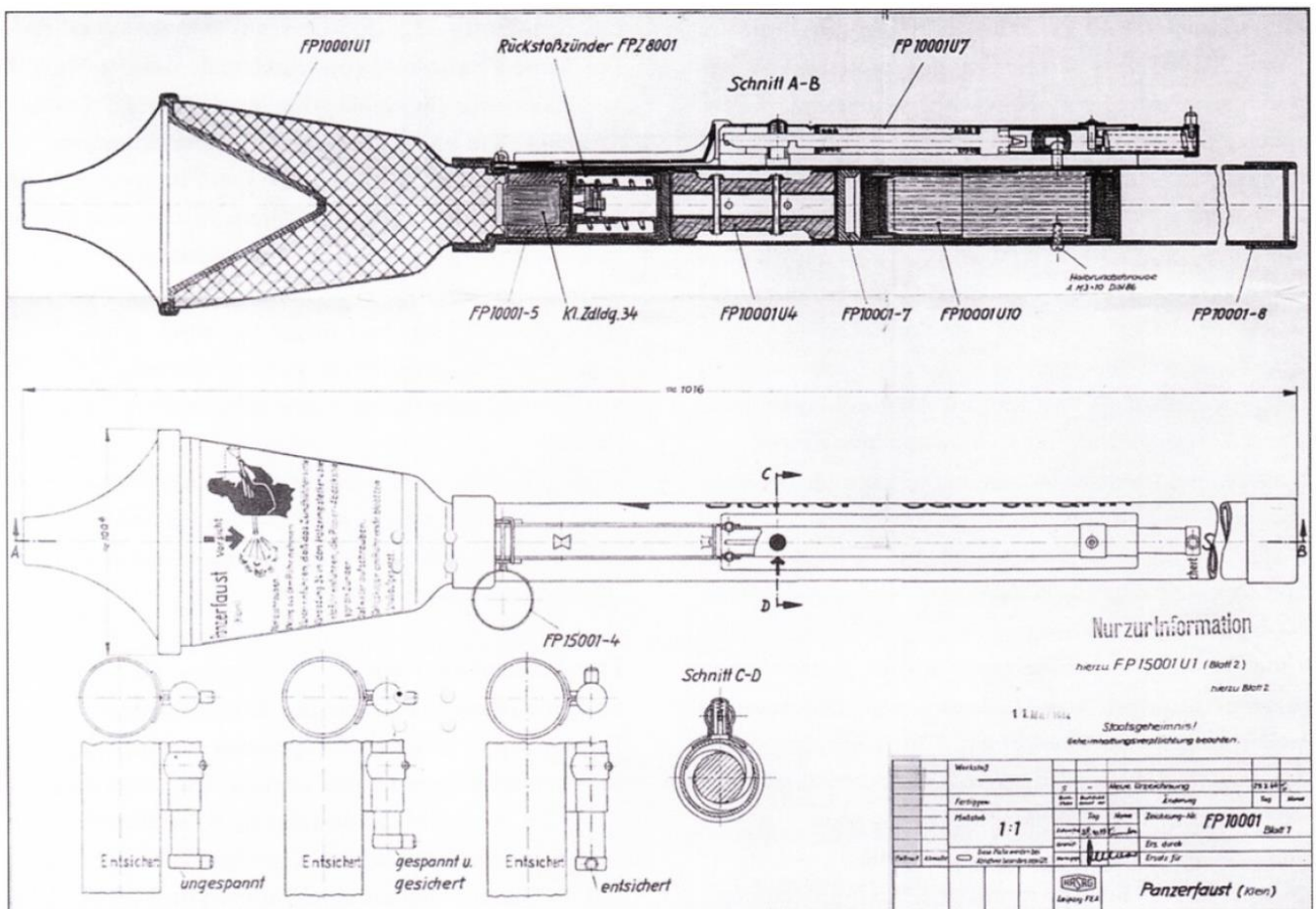

Figure 3.2 Drawing of Panzerfaust 30 (klein) HEAT system [41,50]

The blast overpressure inside an AFV or structure penetrated by a Panzerfaust was considerable. There was a significant blast on the outside of the vehicle, but fragmentation from the thin sheet-steel body was minor, as it broke into a few large pieces. It could be devastating to infantrymen riding on - or on foot - near the target tank, however [40].

The total length of the Panzerfaust system (launch tube + projectile) was 1016 mm, with a tube diameter of 100 mm. Nipple shaped cap in front of the warhead provided a stand-off distance of 65 mm [41]. This nose cap was prone to glancing off sloped armour without detonating which was corrected on Panzerfaust 30 (groß) using blunt nose to ensure more positive initiation [40]. Large number of Panzerfaust 30 (klein) were used by the Romanian Army in 1944 [43]. Also, they were used by armies of Bulgaria, Hungary, Finland, and Italy, as well as occasionally in Allied armies (US army, Soviet army, British army, Polish resistance groups) [40].

The Panzerfaust had an unusual role in trip-wire operated booby traps for tanks during the final stages of the war in NW Europe. A Panzerfaust firing mechanism was attached to a wire that was extended across a road for tanks to use, and when the wire was stretched, the round was fired into the side of the vehicle. Throughout the closing stages of the war, such contraptions slowed the Allied assault in populated regions [38].

During II World war, the shaped-charge weapons were less successful than antitank guns against tanks in open terrain, such as in many sections of the Eastern Front, because of their short range. Nonetheless, the Panzerfaust (and Panzerschreck) were a serious threat to tanks in close terrains like bocage, forests, or cities. The number of US tanks lost during the bocage warfare in June and July 1994 was significantly higher than it was during the pursuit phase of war in August 1944, when Panzerfaust or Panzerschreck strikes only accounted for around 5% of the tanks lost. During the Villiers-Fossard battle, Panzerfaust or Panzerschreck hits caused over 70% of the US tank casualties. British tank losses to Panzerfaust and Panzerschreck hits varied from 6-34% during 1944-1945. The different percentage was due to a number of factors, including the increasing number of Panzerfäuste in the last few months of the war, operations in Germany's urban and forested areas that made it easier to use these weapons, and the sharp drop in the number of German tanks and conventional antitank guns in the last few months of the war [39].

Post-war copies of the Panzerfaust were fielded by two countries, Pansarskott ("armour shot") in Sweden and PAPI ("antitank projectile for infantry") in Argentina. Numerous nations began using single-shot, disposable shoulder-fired rocket launchers in the early 1960s, starting with the US M72-series light anti-tank weapon. The Panzerfaust design had a big impact on these weapons. One round of ammunition packaged, delivered, and issued as a single-round anti-tank weapon immediately proved to have advantages in terms of logistics and the ability of hurried infantrymen to deploy them into battle. Their shelf life is years when packaged in crates with other items. Many nations employed designs similar to 66 mm M72 LAW, with calibers ranging from 58 mm to 105 mm (Soviet Union, Czechoslovakia, Poland, Yugoslavia, China, Sweden, France) [40].

Several of the infantry antitank weapons that emerged after World War II have the Panzerfaust as their ancestor. Soviet anti-tank launchers were the Panzerfaust's most obvious legacy. RPG-1 was an effort to combine the best elements of the German Panzerfaust with the American Bazooka. The RPG-1, in contrast to the Panzerfaust, was built around a reusable launcher, and its projectile was propelled by rockets. The following design, the RPG-2 model, was inspired by the Panzerfaust 150 warhead and had an 80 mm PG-2 warhead (the decrease was made possible by a more effective shaped-charge warhead design). It also had a conical stamped-metal nose cone and a similar safeing and arming mechanism. The PG-2 warhead provided 180 mm depth of penetration while being lighter and smaller. The propellant charge was a part of the PG2 munition, mounted behind the customary tail assembly, because the RPG2 launcher was reusable. The RPG-2 began manufacture in 1949, but its usage by Viet Cong and North Vietnamese troops during the Vietnam War did not become publicly known until the 1960s. The RPG7, a further modification that has since become the most commonly used antitank rocket-propelled grenade launcher in the world, followed it in 1961 [39]. A variety of similar weapons were fielded from the 1950s and well into the 1970s, all owing at least some design features to the Panzerfaust. Examples include the Soviet RPG-16, Chinese Type 70-I, Czechoslovak P27 Pancérovka, Yugoslavian RB M57 and M80, Finnish m/55, all with 44–58 mm launcher tubes and some with over-calibre warheads [40].

4. Numerical simulations

4.1. Introduction

Once the design parameters (for example liner material, geometry, explosive charge), and the important jet parameters (jet tip velocity, jet diameter, and jet breakup time) are known, it is necessary to connect the shaped charge design parameters to the important jet parameters. The penetration performance of a specific shaped charge design can therefore be predicted using the jet parameters as input into one of the penetration models. As a result, the process often has three stages. The collapse of the shaped charge liner is first studied.

The jet formation is then investigated using the findings from the liner collapse. Finally, one makes predictions about penetration depth, hole expansion, and other elements of terminal ballistics using the characteristics of produced jets [2].

In our research, Ansys AUTODYN program was used. Using finite-element, finite-difference, and finite-volume techniques, the hydrocode Autodyn can solve problems that are time-dependent and have geometric and material nonlinearities. Because of the hydrodynamic behavior under high pressures, the term "hydrocode" has historical connotations.

Lagrange (for penetration of jet into target) and Euler processors (for jet formation) are used in this research.

The technique utilized by Wilkins (1973) in the HEMP code serves as the basis for the Lagrange approach in AUTODYN. A structured (I-J-K) numerical mesh of quadrilateral (2D) or brick-like elements (3D) is used by the Lagrange processor. The mesh's vertices move with the speed of the material flow. Compared to the Eulerian technique, the Lagrange formulation is computationally faster as no transport of material across the mesh needs to be estimated. Moreover, the Lagrange framework generally makes it simpler to understand material interfaces, free surfaces, and history dependent material behavior. Lagrange's approach main drawback is that if there is too much material movement, the numerical mesh might get severely deformed, which results in an erroneous and ineffective solution. Additionally, this might ultimately result in the calculation being stopped. One solution to the mesh distortion issue is to rezone the numerical mesh by remapping the deformed solution onto a more regular mesh. To further extend the Lagrange formulation to severely deformed phenomena, AUTODYN also offers additional techniques like erosion. The conservation of mass, momentum, and energy is expressed in Lagrangian coordinates in the partial differential equations that must be solved in the Lagrange processor. These, together with a material model and a set of initial and boundary conditions, define the complete solution of the problem [32].

The series of calculations for a Lagrange discretisation are shown in Figure 4.1.1 for each time step. The forces for the inner zones that were computed in the previous time step are coupled with the updated boundary and/or interaction forces first. The nodal accelerations can be calculated using the momentum equation. The nodal velocities and displacements result from further integration. In Lagrange models, the mesh moves and changes shape along with the material. As a result, the new velocities and displacements can be used to immediately calculate the new volumes and strain rates.
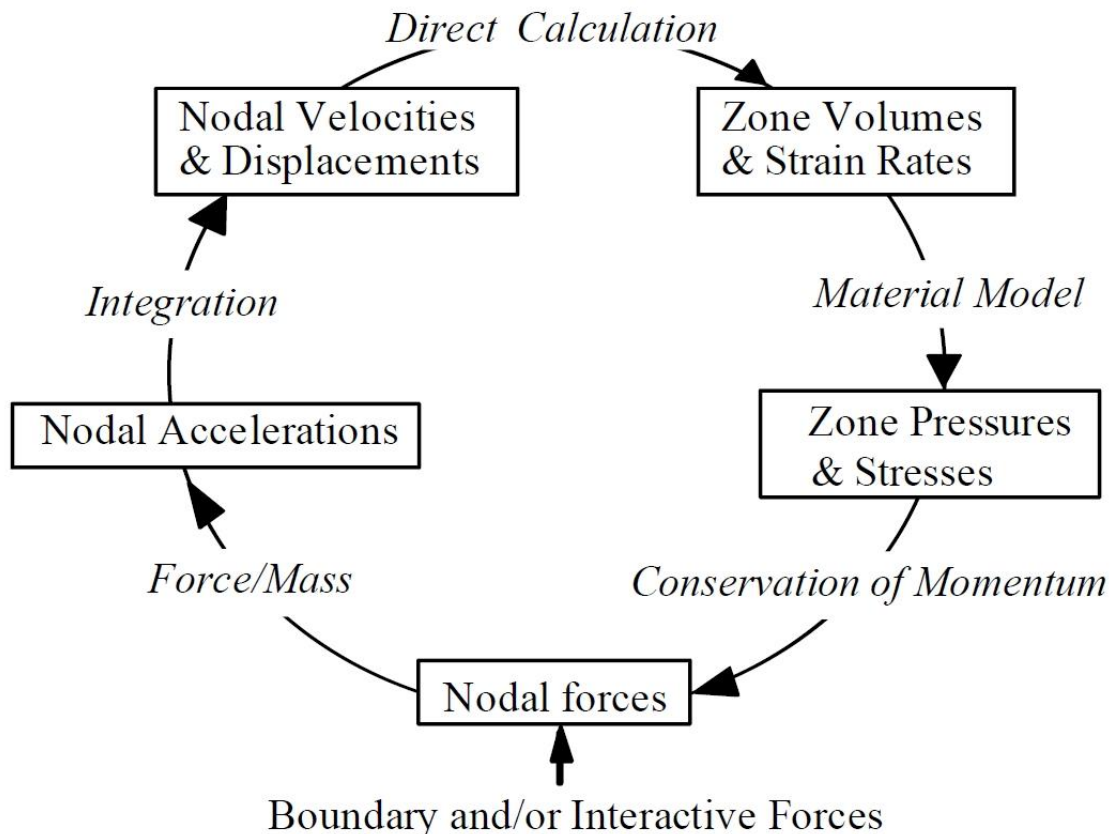

Figure 4.1.1 Lagrange computational cycle [32]

Because of its inherent efficiency, the Lagrange processor is typically used when the deformations and boundary conditions permit.

But Eulerian strategy is more effectively used to manage significant deformations and fluid and gas dynamics (Figure 4.1.2). Hancock's methodology (1976) is the foundation of AUTODYN's initial first-order approach concept. AUTODYN has introduced two different higher order Eulerian schemes. Using Van Leer-developed methods, the Godunov multi-material with strength higher order processor was created. The Zalesak (1979) method, which was based on the earlier operator split algorithms by Boris & Book, is the foundation for the FCT higher order single material Euler processor. Currently, different needs are being served by different Euler processors. For problems involving fluid structure and gas-structure interaction, the first-order scheme is employed. For calculations that are only focused on fluid and gas dynamics or highly distorted structural materials, the multi-material Godunov second-order approach is employed. For single material gas dynamic issues, the FCT approach is employed. The equations governing the conservation of mass, momentum, and energy are solved using the control volume approach in the Euler solvers. To produce precise and reliable solutions, the integral and discrete forms of these equations are stated in conservation form. Lagrangian or transport terms are classified into two classes according to how they affect conserved variables. The finite-difference equations are resolved numerically in two steps. The equations' Lagrangian form is updated or moved forward one time interval in the first step, called the Lagrange step. The updated variables are mapped into the Euler mesh in the second step, known as the Euler step. Several materials are handled using either the Youngs (1982) developed interface technique or the volume fraction technique. Each variable is centered in a cell. This makes it possible to compute fluid-structure or gas-structure interaction problems by forming control volumes of any shape at the intersection of the Euler and Lagrange grids. Large deformations and fluid flow are best handled by an Euler formulation. Tracking free surfaces, material interfaces, and history-dependent material behavior, however, is more challenging. Care must also be taken to limit the numerical diffusion associated with the material convection from cell to cell [32].
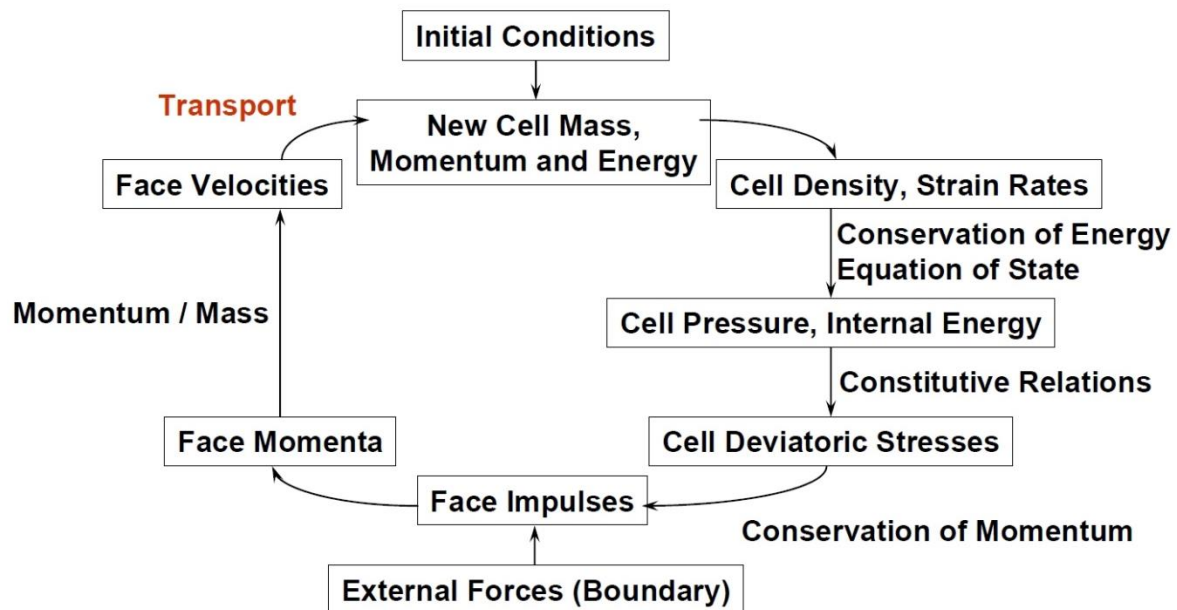

Figure 4.1.2 Euler computational cycle [33]

Advantage of Euler Solver [33] are following: no grid distortions, large deformations possible to handle, mixing of initially separate materials, rezoning not required, erosion not required, higher time step in general. Disadvantages include: more computation time, need finer meshing for similar accuracy, shocks diffused more than Lagrange, less flexible for strength modelling, thin sections require very small time steps.

The following components make up the material model in simulation:
- The equation of state (EOS); represents the connection between pressure, density, and specific energy. It is the stress tensor hydrostatic component, and all three normal stresses are identical under hydrostatic loading.
- Strength model, which calculates the shear resistance of a material. The yield criteria, which depends on material parameters like strain, strain rate, and/or energy, represents relationship of an elastic and plastic regime transition.

- The failure model is often added to the material because the material cannot endure tensile stresses that are higher than their tensile limit. A critical variable for a flow (for example pressure or effective plastic strain) can be used in the failure model to predict when the fracture will start to occur.

The substantial distortion of the Lagrange grid can be solved through the use of erosion algorithm. Here, when a strain reaches a certain threshold, the element is usually removed from the model.

4.2. Setup of numerical simulations

a. Processors and mesh setup

The Euler and the Lagrange approaches were used in this study to form jets and for jets to penetrate steel target, respectively. In the initial analysis, the Euler multi-material part is filled with the explosive charge, the casing, and the liner materials in order to simulate jet formation, following the research presented in [10]. As there are significant distortions due to the high strain rate, the Euler processor is appropriate for the jet formation study. If a Lagrange solver is chosen for the jet formation, the solver would stop working due to large distortions. Until the point of impact with the target, the jet moves through the Euler grid. A Lagrangian mass with a non-uniform velocity distribution is then remapped as the generated jet. The output of these initial simulations was then used as the input for jet penetration into steel target using Lagrange method.

In jetting analysis (Euler approach), the mesh size of 0.25×0.25 mm was used in all simulations (Figure 4.2.1) - which makes 190400 cels for Euler numerical domain. This mesh size is appropriate for jetting analysis [5,10] since it provides accurate solutions within a reasonable calculation timeframe. Generally, by increasing the mesh size (faster calculation times), jet velocity becomes asymptotically smaller during simulations of jet formation process [10].
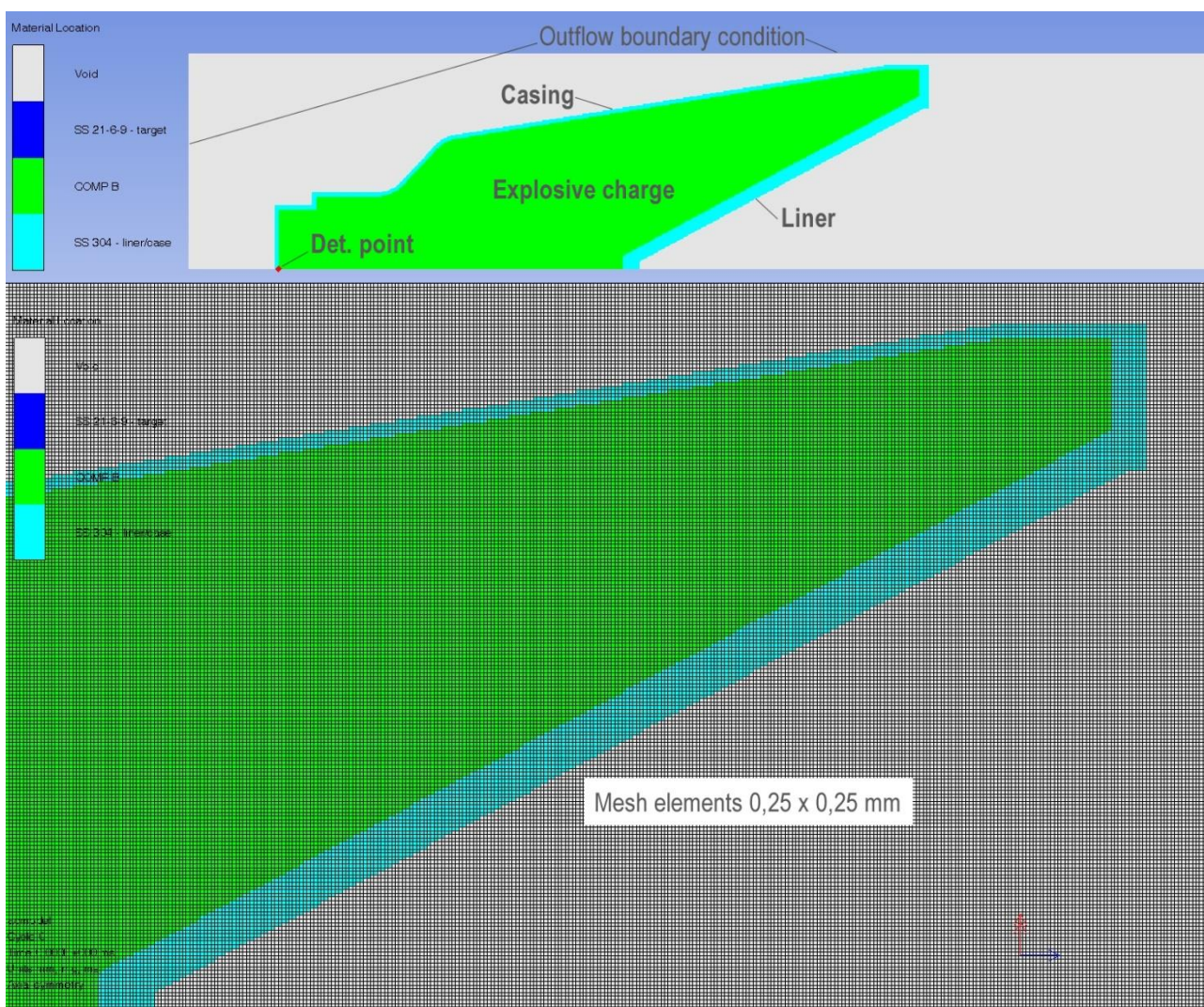

Figure 4.2.1 Euler mesh used in jetting analysis

In penetration analysis (Lagrange approach), the mesh size of 0.5×0.5 mm (both for jet and target) was chosen in simulations (Figure 4.2.2) - which makes 103600 cels for Lagrange numerical domain. Penetration (Lagrange approach) simulations lasted significantly longer than jet formation simulations (Euler solver; run time approximately 2 h), approximately 10h (CPU with 16 processors). Chosen mesh size is appropriate for penetration analysis of shaped charge jet [10]. Generally, by increasing the mesh size, penetration depth of shaped charge jets becomes asymptotically smaller [10].
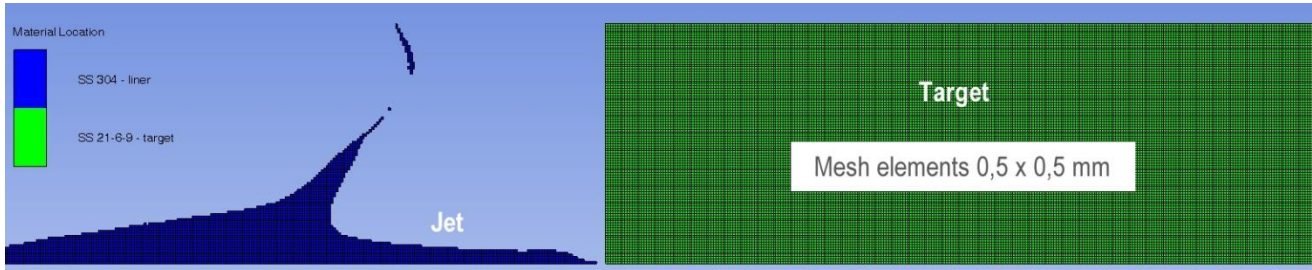

Figure 4.2.2 Lagrangian mesh used in shaped charge penetration analysis

If a corrective measure is not taken in numerical simulations, some Lagrangian cells during the computation may become severely deformed and may impede the progress of the calculation. Hence, if a pre-defined strain (either instantaneous geometric strain, incremental geometric strain, or effective plastic strain) exceeds a certain limit, procedures are implemented into AUTODYN to eliminate such cells from the calculation. The mass inside a cell can either be discarded or distributed to the cell's corner nodes when a cell is thus eliminated from the calculating process. This discard procedure is known as erosion. Generally, this is not true modeling of physical phenomena, but a numerical palliative introduced to overcome the problems associated with the mesh distortions caused by gross motions of a Lagrangian grid [32]. In our research, pre-defined instantaneous geometric strains of 2 and 2 for target and liner, respectively, were chosen in simulations for all materials.

b. Boundary conditions

In the jetting analysis, an Outflow boundary condition was utilized [10] on all numerical domain borders except the symmetry axis (Figure 4.2.1), which allowed the casing material and detonation products to spread toward the Euler part boundary and prevented them from returning to avoid their impact on the development of the jet and slug. In penetration analysis, a Clamp boundary condition (general 2D velocity equals zero) was used on the target (outer edge).

c. Material modeling

Materials used in the research were steel 21-6-9 (target), steel SS 304 for original liner and casing, and for other liners: tungsten alloy with 4% nickel and 2% iron (W4Ni2Fe), molybdenum (Mo), nickel (Ni), oxygen-free high thermal conductivity copper (Cu-OFHC), tantalum (Ta), aluminum alloy (Al 7075-T6), an alloy of gold with 5% copper (Au5Cu), platinum (Pt), an alloy of depleted uranium with 0,75% titanium (U.75Ti), silver (Ag), lead (Pb), depleted uranium alloy with 5% molybdenum (U5Mo), and titanium (Ti).

The local conservation of mass, momentum, and energy is expressed by AUTODYN using differential equations that describe the motion of materials. In addition to the initial and boundary conditions given, another relationship between the flow variables is required to provide a complete solution. It makes use of a material model that connects internal energy, deformation, and stress. The three normal stresses are equivalent, and there are two parts to the stress tensor: a uniform hydrostatic pressure and a stress deviatoric tensor that measures the material's resistance to shear distortion. The relationship between local density (or specific volume), local specific energy (or temperature), and hydrostatic pressure is known as an equation of state (EOS) [32].

In simulations, shock EOS was used for liner materials. The Rankine-Hugoniot equations for shock jump conditions can be viewed as a relationship between any two of the variables: pressure (p), density (ρ), energy (e), shock velocity (U), particle velocity (u_p). In many dynamic experiments, making measurements of u_p and U, it has been found that for most solids and many liquids over a wide range of pressure there is an empirical linear relationship between these two variables [32]:

$$U = c_0 + s u_p \qquad\qquad 4.2.1$$

In expression 4.2.1, c_0 is the sound velocity for given material, and s is material constant representing the slope of U-u_p curve (table 4.2.1). Mie-Gruneisen form of the equation of state, based on the shock Hugoniot is [32,45]:

$$p = p_H + \Gamma \rho \ (e - e_H) \qquad\qquad 4.2.2$$

where Γ is Gruneisen coefficient (with values between 1 and 3 mentioned in literature; it can be approximated with $\Gamma \approx 2s - 1$).

The Hugoniot pressure (p_H) and energy (e_H) are:

$$p_H = \frac{\rho_0 c_0^2 \mu (1 + \mu)}{[1 - (s-1)\mu]^2} \qquad\qquad 4.2.3$$

$$e_H = \frac{1}{2}\frac{p_H}{\rho_0}\left(\frac{\mu}{1+\mu}\right) \qquad\qquad 4.2.4$$

where $\mu = (\rho/\rho_0) - 1$.

Data for this equation of state can be found in various references and many of the materials are available in AUTODYN explicit material library (table 4.2.1). The reference temperature for shock EOS, adopted in simulations, was 295.15 K (default choice in the program).

Table 4.2.1 Shock EOS data for 15 different materials used in simulation (AUTODYN material library)

Material	Density (g/cm^3)	Gruneisen coeff.	c_0 (m/s)	s	Specific heat (J/kgK)
SS 21-6-9 (target)	7.795	1.93	4440	2.2	426
SS 304 (liner/casing)	7.9	1.93	4570	1.49	423
W4Ni2Fe (liner)	18.167	1.67	4030	1.237	143
Mo (liner)	10.2	1.59	5143	1.255	243
Ni (liner)	8.9	1.93	4650	1.445	401
Cu-OFHC (liner)	8.93	2.02	3940	1.489	383
Ta (liner)	16.69	1.67	3410	1.2	135
Al 7075-T6 (liner)	2.804	2.2	5200	1.36	848
Au5Cu (liner)	18.1	2.99	3050	1.56	141
Pt (liner)	21.44	2.74	3640	1.54	128
U.75Ti (liner)	18.62	2.32	2567	1.619	111
Ag (liner)	10.49	2.4	3270	1.55	233
Pb (liner)	11.34	2.74	2006	1.429	124
U5Mo (liner)	18.17	2.32	2590	1.56	114
Ti (liner)	4.51	1.23	5020	1.536	500

In simulations, JWL EOS (used to describe the pressure-volume-energy behaviour of detonation products involving metal acceleration) was used for explosive charge material. Jones, Wilkins, and Lee proposed the equation of state using the following equation to describe the detonation product expansion for high-energy explosive materials [32,45,46,47]:

$$p = A\left[1 - \left(\frac{\omega}{r_1 V}\right)\right]\cdot e^{-r_1 V} + B\left[1 - \left(\frac{\omega}{r_2 V}\right)\right]\cdot e^{-r_2 V} + \frac{\omega E}{V} \qquad\qquad 4.2.5$$

The values of the linear coefficients A and B, as well as nonlinear coefficients r_1, r_2, and ω for many explosives have been determined from comparison of EOS calculations with experimental data (cylinder test - expansion of a hollow metal cylinder filled with explosive and detonated), and are available in AUTODYN material library (table 4.2.2).

Parameter E from expression 4.2.5 is the detonation energy per unit volume, and V represents the ratio of detonation products volume to the volume of undetonated HE charge ($V = V/V_0$). Parameter V can also be expressed using densities as variables.

Values of JWL constants (and other important data) for high explosives can also be found in other various references [46,47].

Table 4.2.2 The JWL EOS parameters for explosive charge studied (AUTODYN material library)

Parameter	Explosive charge (Comp. B)
Density (g/cm^3)	1.717
Parameter A (kPa)	$5.2423 \cdot 10^8$
Parameter B (kPa)	$7.678 \cdot 10^6$
Parameter r_1	4.2
Parameter r_2	1.1
Parameter ω	0.34
C-J detonation velocity (m/s)	7980
C-J energy/unit volume (kJ/m^3)	$8.585 \cdot 10^6$
C-J Pressure (kPa)	$2.95 \cdot 10^7$

To incorporate the effects of material strength and resistance to shear distortion into standard numerical hydrodynamic algorithms, Wilkins (1964) originally developed the methodology used in AUTODYN. Working with stress deviators - differences between total stress and uniform hydrostatic pressure - was the method chosen.

When material strength effects were first conceptualized, materials were thought to be perfectly plastic and elastic. Without overly complicating the computations, it is easy to generalize the strategy by making the yield function dependent on material characteristics like strain, strain rate, energy, temperature, etc.

Several of these more sophisticated treatments have been implemented in the AUTODYN library, among them Steinberg-Guinan, Mohr-Coulomb, Johnson-Cook, Zerilli-Armstrong, Piecewise-linear, Johnson-Holmquist etc. Some authors neglect the strength effects of liner material in simulations because shock pressures developed are much higher than material strength [10].

In simulations, the liner, casing, and target materials were all subjected to the Steingerg-Guinan strength model. Their model includes formulas for the shear modulus G and yield strength Y as functions of internal energy (temperature), effective plastic strain, pressure, and constants for various metals. Their computer calculations have been able to replicate the measured stress and free-surface velocity vs time data for several shock wave investigations using the model.

The values of these parameters are all in the AUTODYN library (table 4.2.3) and they were used in simulations. In Steingerg-Guinan strength model, the constitutive relations for shear modulus and yield stress for high strain rates are [32,48]:

$$G = G_0 \cdot \left[1 + \left(\frac{G_p^{'}}{G_0} \right) \frac{p}{\eta^{1/3}} + \frac{G_T^{'}}{G_0} (T - 300) \right] \qquad 4.2.6$$

$$Y = Y_0 (1 + \beta \varepsilon)^n \left[1 + \left(\frac{Y_p^{'}}{Y_0} \right) \frac{p}{\eta^{1/3}} + \frac{G_T^{'}}{G_0} (T - 300) \right] \qquad 4.2.7$$

subject to $Y_0 (1 + \beta \varepsilon)^n \leq Y_{max}$, where ε is effective plastic strain, T - temperature (K), $\eta = V_0/V$ (compression), β and n are work hardening constants. Primed parameters with the subscripts p and T are derivatives of that parameter with respect to pressure and temperature at the reference state (T = 300 K, p = 0, ε = 0). The subscript zero refers to values of G and Y at the reference state.

The work-hardening function $(1 + \beta \varepsilon)^n$ from 4.2.7 is a semi-empirical one that best fit the data for studied metals.

Parameter Y_{max} is the largest value for Y found in the literature. At high stress, the effect of P and T on Y can be more important than work hardening. For example, aluminum shocked to 41.2 GPa shows that the combined effect of P and T is to increase Y by a factor of 3, while work hardening only increases Y by 37% [48].

The values of Steingerg-Guinan parameters for several materials can be found in the AUTODYN library (table 4.2.3) and also in [48].

Table 4.2.3 Steinberg-Guinan strength model parameters for materials studied (AUTODYN material library)

Material	Shear modulus (kPa)	Yield stress (kPa)	Maximum yield stress (kPa)	Hardening constant	Hardening exponent	Derivative dG/dP	Derivative dG/dT (kPa/K)	Derivative dY/dP	Melting temp. (K)
SS 21-6-9 (target)	$7.7 \cdot 10^7$	$6.8 \cdot 10^5$	$2.5 \cdot 10^6$	35	0.23	1.74	$-3.504 \cdot 10^4$	0.01537	$2.38 \cdot 10^3$
SS 304 (liner/case)	$7.7 \cdot 10^7$	$3.4 \cdot 10^5$	$2.5 \cdot 10^6$	43	0.35	1.74	$-3.504 \cdot 10^4$	0.007684	$2.38 \cdot 10^3$
W4Ni2Fe (liner)	$1.45 \cdot 10^8$	$1.87 \cdot 10^6$	$4 \cdot 10^6$	7.7	0.13	1.494	$-2.204 \cdot 10^4$	0.01926	$2.263 \cdot 10^3$
Mo (liner)	$1.25 \cdot 10^8$	$1.6 \cdot 10^6$	$2.8 \cdot 10^6$	10	0.1	1.425	$-1.9 \cdot 10^4$	0.01824	$3.66 \cdot 10^3$
Ni (liner)	$8.55 \cdot 10^7$	$1.4 \cdot 10^5$	$1.2 \cdot 10^6$	46	0.53	1.3936	$-2.787 \cdot 10^4$	0.002282	$2.33 \cdot 10^3$
Cu-OFHC (liner)	$4.77 \cdot 10^7$	$1.2 \cdot 10^5$	$6.4 \cdot 10^5$	36	0.45	1.35	$-1.798 \cdot 10^4$	0.003396	$1.79 \cdot 10^3$
Ta (liner)	$6.9 \cdot 10^7$	$7.7 \cdot 10^5$	$1.1 \cdot 10^6$	10	0.1	1.001	$-8.97 \cdot 10^3$	0.01117	$4.34 \cdot 10^3$
Al 7075-T6 (liner)	$2.67 \cdot 10^7$	$4.2 \cdot 10^5$	$8.1 \cdot 10^5$	965	0.1	1.74	$-1.645 \cdot 10^4$	0.02738	$1.22 \cdot 10^3$
Au5Cu (liner)	$3.07 \cdot 10^7$	$6.3 \cdot 10^5$	$1.1 \cdot 10^6$	1000	0.072	1.2	$-1.001 \cdot 10^4$	0.02463	$1.88 \cdot 10^3$
Pt (liner)	$6.37 \cdot 10^7$	$3 \cdot 10^4$	$3.4 \cdot 10^5$	1300	0.19	1.599	$-8.982 \cdot 10^3$	$-7.53 \cdot 10^{-4}$	$2.84 \cdot 10^3$
U.75Ti (liner)	$7.4 \cdot 10^7$	$9.5 \cdot 10^5$	$2.2 \cdot 10^6$	1000	0.095	4.351	$-5.802 \cdot 10^4$	0.05586	$1.71 \cdot 10^3$
Ag (liner)	$2.98 \cdot 10^7$	$5 \cdot 10^4$	$6.6 \cdot 10^5$	28	0.8	1.401	$-1.299 \cdot 10^4$	0.00235	$1.604 \cdot 10^3$
Pb (liner)	$8.6 \cdot 10^6$	$8 \cdot 10^3$	$1 \cdot 10^5$	110	0.52	1	$-9.976 \cdot 10^3$	$-9.3 \cdot 10^{-4}$	$0.760 \cdot 10^3$
U5Mo (liner)	$3.5 \cdot 10^7$	$8.5 \cdot 10^5$	$1.68 \cdot 10^6$	250	0.25	1.201	$-1.001 \cdot 10^4$	0.02916	$1.82 \cdot 10^3$
Ti (liner)	$4.34 \cdot 10^7$	$8.5 \cdot 10^5$	$1.45 \cdot 10^6$	210	0.1	0.499	$-2.699 \cdot 10^4$	0.009775	$2.26 \cdot 10^3$

A popular simplification in AUTODYN is to simulate jet formation in the absence of air, using option Void. One less material needs to be included in the model for simulating the jet formation, which means fewer computations are required. One disadvantage of creating a jet in a vacuum (Void) as opposed to air is that the air drag force brought on by a jet's movement through the air cannot be modeled. Gürel [5] found there is no significant difference in jet tip velocities in the range of 1 to 3 CD (charge diameter) standoff distance when using Void instead of air in simulations. Since the Panzerfaust 30 (klein) warhead had stand-off distance of 65 mm (0,68 CD), option Void is used throughout simulations for faster calculation times.

4.3. Validation of a numerical model

Verification and validation procedures are, in general cases, used to assess numerical models by estimating uncertainties and inherent errors. Verification involves examining and documenting the input parameters for geometry, initial and boundary conditions. Mesh sensitivity studies can also be carried out to limit errors, regardless of whether they are the result of inadequate spatial discretizations, excessive temporal advancement, or coding problems linked to discrete approximations of the partial differential equations. Verification can also include comparison with an analytical solution (ie. comparing numerical solution for several meshes with proven analytical solution).

On the other hand, validation is a process for assessing numerical simulation model uncertainty by using available experimental data and comparing them [34]. Throughout the code's development process and through the use of many authors, AUTODYN program was thoroughly verified in various ballistics applications (for example [49]).

In this research, validation of the numerical model was performed using test data for penetration depth [38,39,40,44] and radius of the entry hole [40] for Panzerfaust 30 (klein) warhead. The numerical simulation

setup was the same as described in Section 4.2. For validation of this original Panzerfaust 30 (klein) warhead model, following materials were used: composition B for explosive charge (table 4.2.2), steel (SS 304) for liner and casing (tables 4.2.1 and 4.2.3), and steel (SS 21-6-9) for a target (tables 4.2.1 and 4.2.3).

SS 21-6-9 (material chosen in simulations for the target) is nitrogen-strengthened austenitic stainless steel with high manganese content. Thanks to its high mechanical strength, steel 21-6-9 is primarily used for the manufacturing of components in the aircraft industry. Proof strength $R_{p0.2}$ (@ 20 °C), hard condition (steel that has been given heat treatment and then quenching followed by tempering), for this steel is ≥ 827 MPa, and tensile strength R_m (@ 20 °C), hard condition, is ≥ 979 MPa [51].

SS 304 (material chosen for the liner) is austenitic grade steel that can be severely deep drawn. It is the most versatile and widely used stainless steel, alloyed with 18% chromium and 8% nickel. Proof strength is min. 210 MPa, and tensile strength 520-720 MPa [52].

Figure 4.3.1 shows the geometry (2D CAD drawing) of the initial numerical setup of Panzerfaust 30 (klein) warhead and target, with dimensions provided. Dimensions were adopted from a technical drawing of this munition (Figure 3.2).
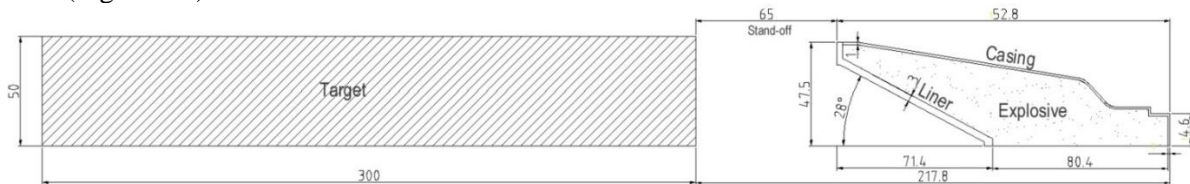

Figure 4.3.1 Geometry of initial setup (Panzerfaust 30 (klein) warhead and target)

Figure 4.3.2 shows the distribution of jet and slug velocity (contours; unit m/s) at the moment of impact (35 μs) into a target (3D model made by rotating 360° around symmetry axis) 2D axisymmetric model around x-axis). The maximum jet tip velocity at this moment was 6415 m/s (represents the impact velocity into a target).
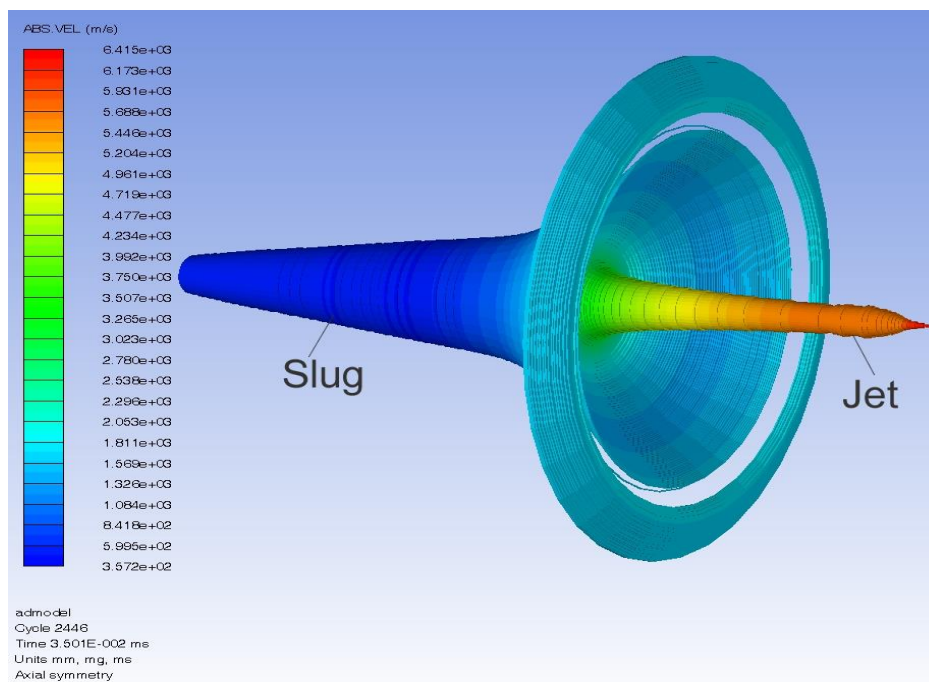

Figure 4.3.2 Distribution of jet and slug velocities (contours) at the moment of impact (35 μs) into target (materials used: composition B for explosive charge, and steel 304 for liner and casing)

Figure 4.3.3 shows sequences of shaped charge jet formation process during different timeframes (15, 20, 15, 30 and 35 μs) with velocity contours shown. Non-uniformity of velocity throughout liner material can be noticed. This causes the jet to stretch and eventually break up (this also contributes to density gradient along the jet). It can also be seen that the jet is significantly faster than slug which follows it. Maximum jet velocity obtained from simulations for this (original warhead) case was 6595 m/s, at 22 μs (from the initiation of charge).
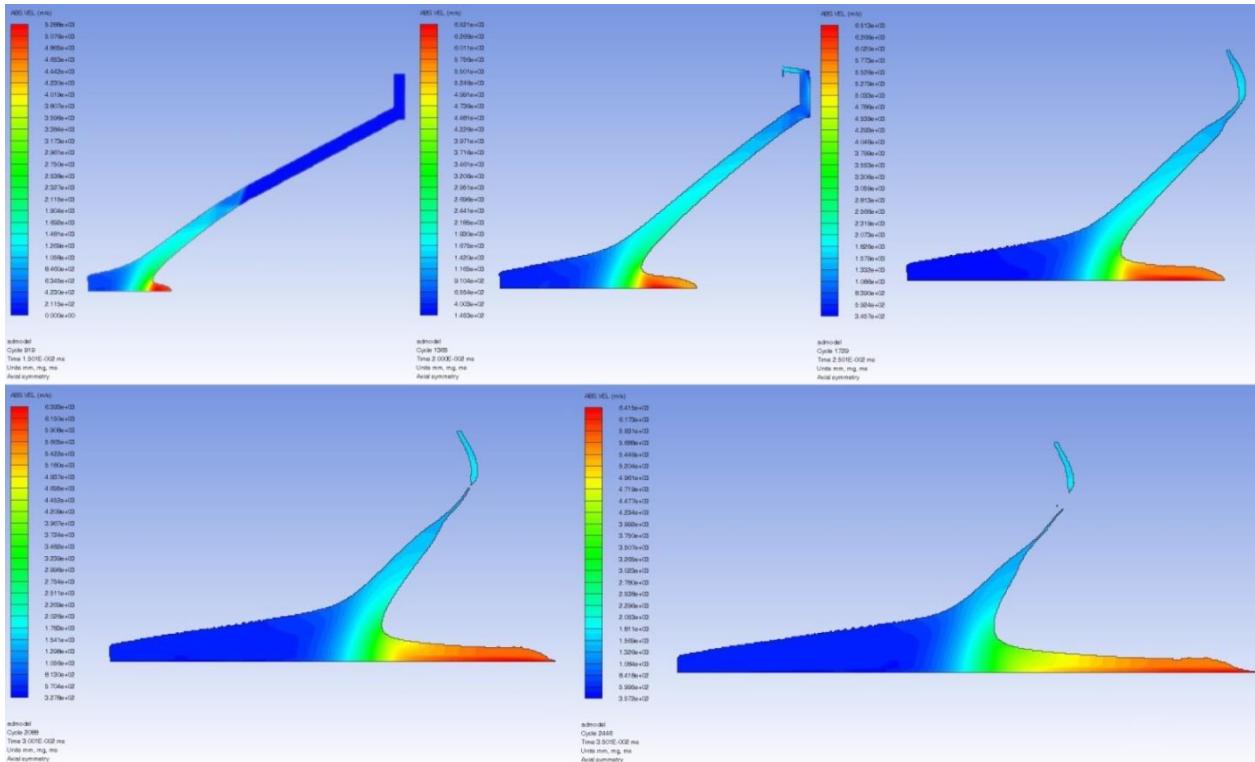
Figure 4.3.3 Sequences of jet formation (2D axisymmetric upper half of liner shown) during different timeframes (15, 20, 15, 30 and 35 μs) with velocity contours shown

Figure 4.3.4 shows pressure contours (with equal scale used) during the process of liner collapse, for different timeframes. Shockwave moving through the explosive charge can be seen, as well as wave reflections inside the warhead. The maximum pressure achieved in the warhead was around 38 GPa (at the points of contact between the shockwave and liner).
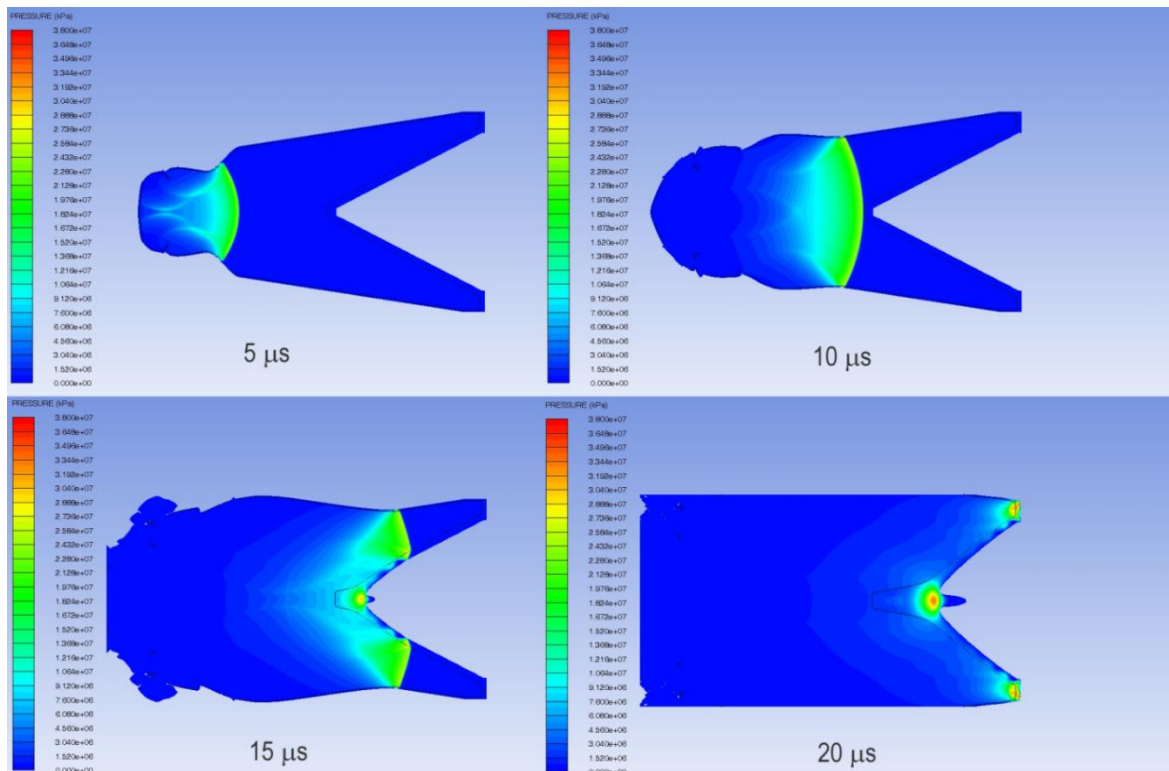

Figure 4.3.4 Pressure contours during the process of liner collapse
(materials used: composition B for explosive charge, and steel 304 for liner and casing)

Figure 4.3.5 shows the penetration depth of the shaped charge jet (SS 304) into a target (SS 21-6-9), using the

Lagrange approach. The depth of penetration achieved (using the simulation) was 140.12 mm, which matches the experimental data (140 mm).

The cut-off jet velocity for this case (original Panzerfaust 30 (klein) warhead) was approximately 1765 m/s. Broadly speaking, higher-density materials (for example tungsten, gold) have lower cut-of velocities. In Figure 4.3.5, a shaped charge slug can be seen located deeper inside the target after the penetration process is finished. This happens because the material (steel) has a relatively low density (compared for example to tungsten). Later on in the research, it will be shown that higher-density liner materials generally form the slug which cannot fully enter the penetration hole, and can be found stuck at the entry of a hole.
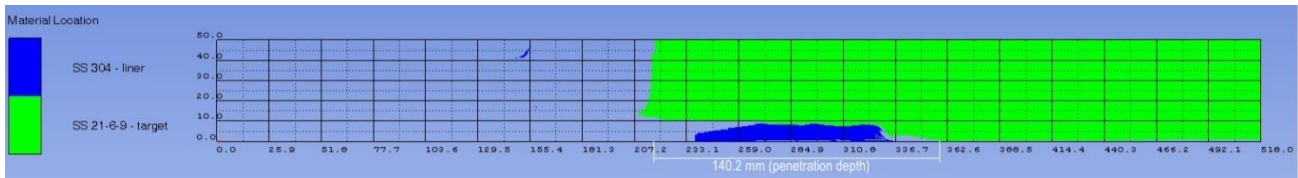

Figure 4.3.5 Penetration depth of the original warhead shaped charge jet (SS 304) into a target (SS 21-6-9), using the Lagrange approach

Exact penetration depth (shown in Figure 4.3.5) was determined using the program Graph extract, where axes were accordingly calibrated, and then penetration depth was determined (Figure 4.3.6). To precisely calculate penetration depth into steel target, a value obtained in Graph extract, shown in Figure 4.3.6 (358 mm), had to be subtracted with value 217,8 mm (see Figure 4.3.1) which represents a distance of target frontal part from the origin of coordinate system positioned at the end of warhead).
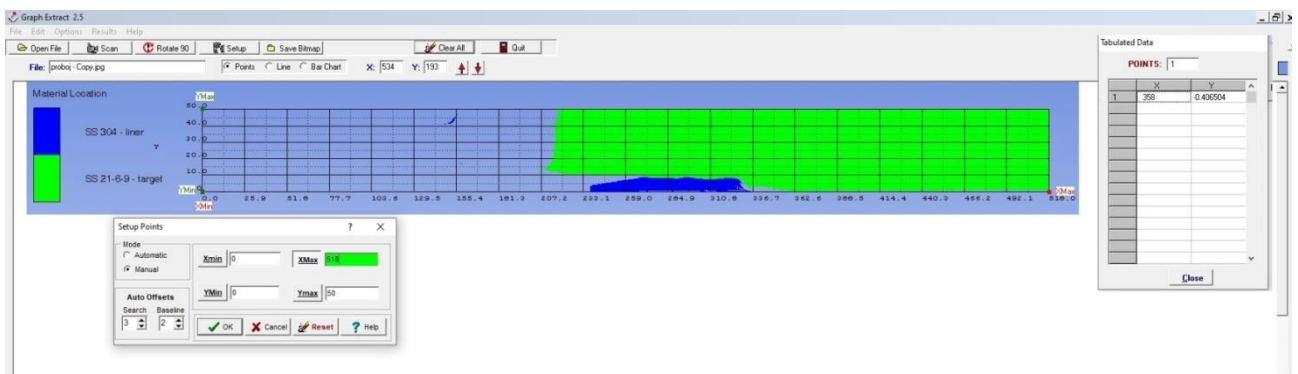

Figure 4.3.6 Precise determination of penetration depth of the original warhead shaped charge jet (SS 304) into a target (SS 21-6-9), using Graph extract program

Max. diameter of target entry hole was little bit larger than 20 mm (Figure 4.3.7), which is in accordance with available literature data for this warhead (the entry holes for Panzerfaust warhead were typically 25-38 mm in diameter and the exit hole could be as small as 13 mm wide [40]). A lip formation can be seen at the entry hole, which is related to the significant energy transfer occurring at impact. The kinetic energy of the jet plays a major role in the energy transfer throughout the penetration process, and significant thermal impacts were not observed on the target plate.
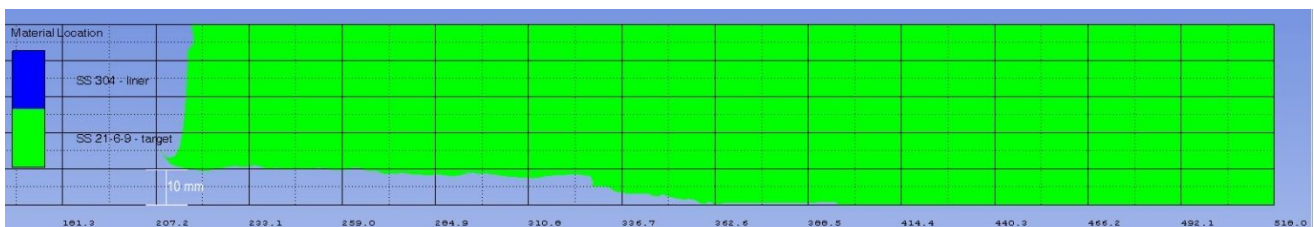

Figure 4.3.7 Exact determination of penetration depth of the original warhead shaped charge jet (SS 304) into a target (SS 21-6-9), using Graph extract program

Results obtained for original Panzerfaust 30 (klein) warhead model will be used next as a comparison baseline further on in the research, with modifications only applied to the shaped charge liner materials (table 4.2.3) to determine their influence on the formation process and penetration depth (relative increase/decrease compared to the original liner).

4.4. Influence of different liner materials on jet formation process and penetration depth

Materials used in numerical simulations to determine the influence of liner materials on the jet formation process and penetration depth into steel targets are presented in tables 4.2.1 and 4.2.3 (shock EOS and Steinberg-Guinan models; these parameters, which deviate from the commonly found and published speeds of elastic sound, are fitted from shock velocity data and are relevant for the current study because they are based on high-pressure shock conditions).

Liner materials are chosen based on literature recommendations [1,14,63] and availability in the AUTODYN materials database. The numerical setup was the same as the one described in Section 4.2, with only the difference in the liner materials chosen. Simulations are finished when no further change in penetration depth is obtained by further marching through time.

Table 4.4.1 summarizes important parameters obtained from numerical simulations (max. jet velocity obtained, penetration depth, penetration depth percentual increase/decrease compared to the original liner (SS 304), and a ranking of potential liner materials based on penetration depth obtained).

Table 4.4.1 Characteristics of different liner materials and parameters obtained from numerical simulations, with the ranking of materials provided based on penetration depth results

Liner material	Max. jet velocity (km/s)	Penetration depth (mm)	Penetration depth percentual increase/decrease compared to original liner (SS 304)	Ranking of materials based on penetration depth obtained
SS 304	6.595	140.19	-	**11**
W4Ni2Fe	4.481	188.06	34.15	**4**
Mo	5.826	148.24	5.74	**9**
Ni	6.253	153.71	9.64	**7**
Cu-OFHC	6.354	131.19	-6.42	**12**
Ta	4.588	183.79	31.10	**5**
Al 7075-T6	8.493	80.79	-42.37	**14**
Au5Cu	4.727	191.29	36.45	**3**
Pt	4.278	196.09	39.87	**2**
U.75Ti	4.641	176.09	25.61	**6**
Ag	6.106	153.39	9.42	**8**
Pb	6.102	142.43	1.6	**10**
U5Mo	4.685	196.59	40.23	**1**
Ti	7.339	97.29	-30.60	**13**

A shaped charge liner's potential maximum jet velocity while maintaining a coherent jet depends significantly on the sound speed of given material. The resulting jet won't be coherent if the liner is collapsing with a velocity that is faster than the liner material's sound speed. It is known that bulk modulus and density both affect the sound speed of liner material. Jet tip velocity will be increased with a faster collapse velocity, so to increase the kinetic energy of the jet, increased jet tip velocity is always preferred. The maximum achievable jet tip velocity is 2.34 times the bulk sound velocity of the material [8].

The minimal effective jet velocity (cut-off velocity) is influenced by the particulation process (generates tumbling and transverse moving particles), and the precision of the jet (straightness of the jet). Increased jet length is implied by longer particulation periods produced by finer crystal structures. The crystal structure of the raw materials and the method used to produce the liner both affect the crystal structure of the liner material. For a good particulation process, finer and more uniform crystal structures are preferred. The square root of the density of the liner material is proportional to the penetration depth. Lower jet tip velocities are produced by a few metals with higher densities because they have lower sound velocities. But it is generally difficult to manufacture them with the same desirable fine crystal structure as the most often used liner material - copper [8].

It is important to note that materials with high density, high ductility, moderate to high speed of sound, high melting temperature and high dynamic strength are likely to result in better penetration depth.

In the simulations performed, the greatest penetration depth increase was achieved with a liner made of depleted uranium alloy with 5% molybdenum (196.6 mm; 40.2% increase compared to original liner). Generally, depleted uranium is by-product of the production of enriched uranium for use as fuel in nuclear

reactors and in the manufacture of nuclear weapons. It has a lower content of the fissile isotope [235]U than natural uranium. Depleted uranium alloys have desirable properties such as high density, high hardness, and high toughness. Also, they are pyrophoric, which means they can also enhance blast effects. Depleted uranium alloys, along with the low cost of raw materials, have the advantage of easy solubility and relatively easy casting into molds, while in the case of tungsten, it is a more involving and expensive process.

The second greatest penetration increase in simulations was obtained with a platinum liner (196.1 mm; 39.9% increase compared to original liner) even though the jet made of platinum had the lowest max. velocity (4278 m/s). Platinum has the advantage of having the highest density of all chosen materials for liner. Also, platinum is more ductile than gold, silver or copper; in fact it is the most ductile of pure metals. This is also shown in simulations where platinum had the highest jet break-up time of all chosen materials. However, its use is costly since it is an extremely rare metal (obtained commercially as a by-product from nickel and copper mining and processing) and precious metal commodity.

Jet from a gold-copper alloy with 95% gold and 5% copper (Au5Cu) also showed high penetration depth increase (191.3 mm; 36.5% increase compared to the original stainless-steel liner) with comparatively low jet tip velocity (4727 m/s). Gold (together with Al, Cu, Pb, Ni, Pt, Ag, W) has face-centered cubic crystal which contributes to potential high-ductility jets [14]. Compared to other chosen materials, gold has relatively high density, lower sound speed, moderate melting temperature, and good ductility (copper also increases the ductility of an alloy, with a small decrease in density). But, as in the case of platinum, possible military use of gold is too expensive in most cases (gold is approximately 2 times more expensive than platinum [57]).

Tungsten, even though brittle material, is potentially attractive liner material because of its high sound speed and high density (based on standard penetration equation used for shaped charge jets ($P = l_j \sqrt{\rho_j / \rho_t}$), tungsten as a liner material could theoretically provide a 47% deeper penetration than copper [63]). Its strength and brittleness are highly dependent upon temperature and manufacturing process. Tungsten alloys can produce a jet with good ductility. Alloys of W, Ni and Fe are pressed/sintered [14]. Pressed or sintered liners produce a continuous jet of fine particles, but the jet tends to disperse radially at long standoff distances. There is also a degree of variability in the jet quality and charge performance [14]. Porous-shaped charge liners (porous brittle metals are mostly being used in shaped charges for oil well perforation, where the intention is to avoid the creation of a large slug that could block the hole [63]) are generally created by compressing metal powder into a solid structure with an appropriate shape. Liners created in this way - compressing powdered metals - typically contain a composite of two or more different metals, at least one of which is a heavy or higher-density metal, and other powdered metals serve as a binder or matrix. In the past, tungsten, hafnium, bismuth have all been utilized as examples of greater density metals used. Binder or matrix metal can be made of metals with a high degree of malleability and ductility (for example nickel, zinc, tin, uranium, silver, gold, antimony, cobalt, copper, zinc alloys, tin alloys, palladium). When the binder or matrix material has a lower density, the overall density of the shaped charge liner is reduced which somewhat reduces the penetration depth. Using binder or matrix materials with higher sound velocity can also have benefits. Porous liners should generate a coherent and dense jet. They must be made of material that does not shatter into fragments after detonation in order to produce a cohesive jet.

The jet made of tungsten with 4% nickel and 2% iron (W4Ni2Fe) alloy, used in the simulation, had also a significant increase in penetration depth (188.1 mm; 34.2% increase than the original liner). A combination of high density, good ductility, relatively high sound speed and melting temperature makes this alloy a potential candidate for high-performance liners, with adequate manufacturing technology (costs effective process is always desirable). Tungsten bar costs around 50 USD/kg [57].

Next in the line for simulation was jet from tantalum liner which showed an increase in penetration depth of 31.1% compared to the original liner. Tantalum is a candidate liner for many warhead types applications (missiles, torpedoes, submunition). As mentioned in [14], Ta, Mo and W all form coherent and ductile jets when properly designed. The density of tantalum is relatively high, the melting point is extremely high (the highest of chosen materials), with a somewhat lower sound speed. The price of tantalum ore is about $158 USD/Kg of Ta_2O_5 content [58].

An alloy of depleted uranium with 0,75% titanium (U.75Ti) has already been suggested in the research [62], as a potential material for shaped charge liners. Numerical simulations showed (table 4.4.1) that, by using this depleted uranium alloy, an increase in penetration depth of 25.6%, compared to the original liner, can be

obtained. This alloy has high density (second highest among the chosen liner materials), low sound speed (lowest of chosen materials) and low melting point (second lowest of chosen materials). It is known to be pyrophoric which is favorable characteristic (can increase the blast effect). This binary alloy was introduced in the 1970s (it is used for example in the 105 mm M833 and 120 mm M829 APFSDS penetrators). Mechanical characteristics (strength, ductility, fracture toughness, elongation) and phase diagram of this alloy can be found in [60].

Nickel, silver, and molybdenum fared somewhat poorer than above mention liner materials, with a marked increase in penetration depth (compared to the original steel liner) lower than 10%. Nickel, with its low density (compared to other materials chosen for liners), has high sound velocity and intermediate melting temperature and strength. Nickel is a hard, malleable, and ductile metal. Jet from nickel showed an increase in penetration of 9.6%. Nickel is 2-3 times more expensive than copper [57].

Silver has potential as a liner material, primarily because of its extreme ductility. It has intermediate density, with low melting temperature, low sound velocity, and low strength - compared to other liner materials chosen. Jet from silver penetrated 153.4 mm into steel target (9.4% increase compared to original liner). Silver is similar in physical and chemical properties to copper and gold. Ingots of silver cost 750 USD/kg [57].

Molybdenum is also a desirable material for shaped charge liners because of its high ductility (close to high-quality copper), high sound speed and high melting temperature (sixth-highest melting point of any element), as well as moderate density. These characteristics give it a relatively high-velocity jet (molybdenum-shaped charge liners are known to be used in high-speed jet applications). The jet made of molybdenum showed an increase in penetration depth of 5.7% compared to the original liner. As a result of molybdenum's ability to tolerate extremely high temperatures without considerably expanding or weakening, it is useful in environments of intense heat, including armor applications. Molybdenum is occasionally used instead of tungsten because of its lower density and more stable price. Presently, the price of molybdenum is around 75 USD/kg [59].

The lead (Pb) liner showed small increase in penetration depth (1.6%). Lead has the advantage of higher density (than original liner) and ductility, but has the lowest strength, sound speed and melting temperature (this implies easier manufacturing) of all materials chosen. As a potential liner material, lead is inexpensive (around 2.1 USD/kg) but it is toxic, even in small amounts. It is resistant to corrosion and relatively inert.

The copper (OFHC version) jet interestingly showed a somewhat lower penetration depth than the original steel liner, with a recorded decrease of -6.4%. This can be attributed to higher sound velocity, higher strength and higher melting temperature of steel, even though steel has a lower density (around 12%) and lower ductility than copper. Nonetheless, copper is the most frequently used material for shaped charge liners and EFP munition. Copper is a relatively soft, malleable, and very ductile metal. Before failure, the ideal shaped charge jet material experiences substantial plastic deformation and high strain rates. This ensures long, cohesive jets. The oxygen-free copper used in the majority of shaped charge jets can withstand significant deformation before failing. Compared to other materials in this research, copper has relatively low density, sound velocity, melting temperature, and strength. The price of copper is around 4 USD/lb, making it relatively cheap [59]. Compared to stainless steel, copper is more expensive.

The titanium liner showed a significant decrease in penetration depth (-30.6%), and the diameter of the hole in the target obtained with this liner is comparable with that of aluminum liner (Figs. 4.4.1 and 4.4.2). Titanium has high ductility, low density (second lowest after aluminum), high sound speed (second highest after molybdenum), and relatively high melting temperature compared to other materials chosen. Its corrosion resistance and strength-to-density ratio are the highest of any metallic element. Titanium is 60% denser than aluminum, but more than twice as strong. It can be alloyed with iron, aluminum, vanadium, molybdenum and other metals to produce strong, lightweight alloys for aerospace and military applications (for example armor plates). The price of titanium is around 8 USD/kg [57].

The jet formed with the Al 7075-T6 liner attained the highest velocity (6543 m/s) but achieved the lowest penetration depth (80.8 mm; -42.4% decrease comparing to the original liner). This is understandable since aluminum has the lowest density of all chosen materials for liner. However, with this liner, the largest diameter of the hole in the target was obtained. Aluminum is the third most abundant element on Earth after oxygen and silicon. Aluminum is soft, ductile, and malleable allowing it to be easily drawn and extruded. It is also easily machined and cast. Aluminum is frequently used in the military (for example armour on APC and IFV) and aerospace industry where light weight and relatively high strength are crucial.

In practical applications, aluminum is used when a larger crater volume is needed instead of deep penetration or when the target is comparatively softer than usual steel armour. It has good jet ductility and it is pyrophoric so it can be used for enhancing blast effects since it is exothermally reactive. Aluminum has a high chemical affinity to oxygen, which renders it suitable for use as a reducing agent in the thermite reaction. Aluminum is 4 times cheaper than copper [57].

Generally, in real-case scenarios, after the penetration process is finished, the liner slugs can be found deeper inside the target hole, at the hole entry, or in the vicinity of the target (on the ground). Figs. 4.4.1 and 4.4.2 show penetration depths and hole profiles, made with liners of different materials, obtained using simulations. Simulations show that a slug of liners made of lower-density materials (for example Ti, SS 304, Ni, Cu, Al) are found inside the target hole, while slugs of liners with higher-density (W alloy, Mo, Ta, Au, Pt, DU alloys, Ag) are found stuck at the entry hole. It was interesting to note that the lead slug was "destroyed" during the penetration process (Figure 4.1.1) even though lead has a relatively large density. This occurred because lead has the lowest strength of all materials chosen. Jets are completely eroded during the penetration process and cannot be seen in Figs. 4.4.1 and 4.4.2 (which show the final stage of the penetration process).
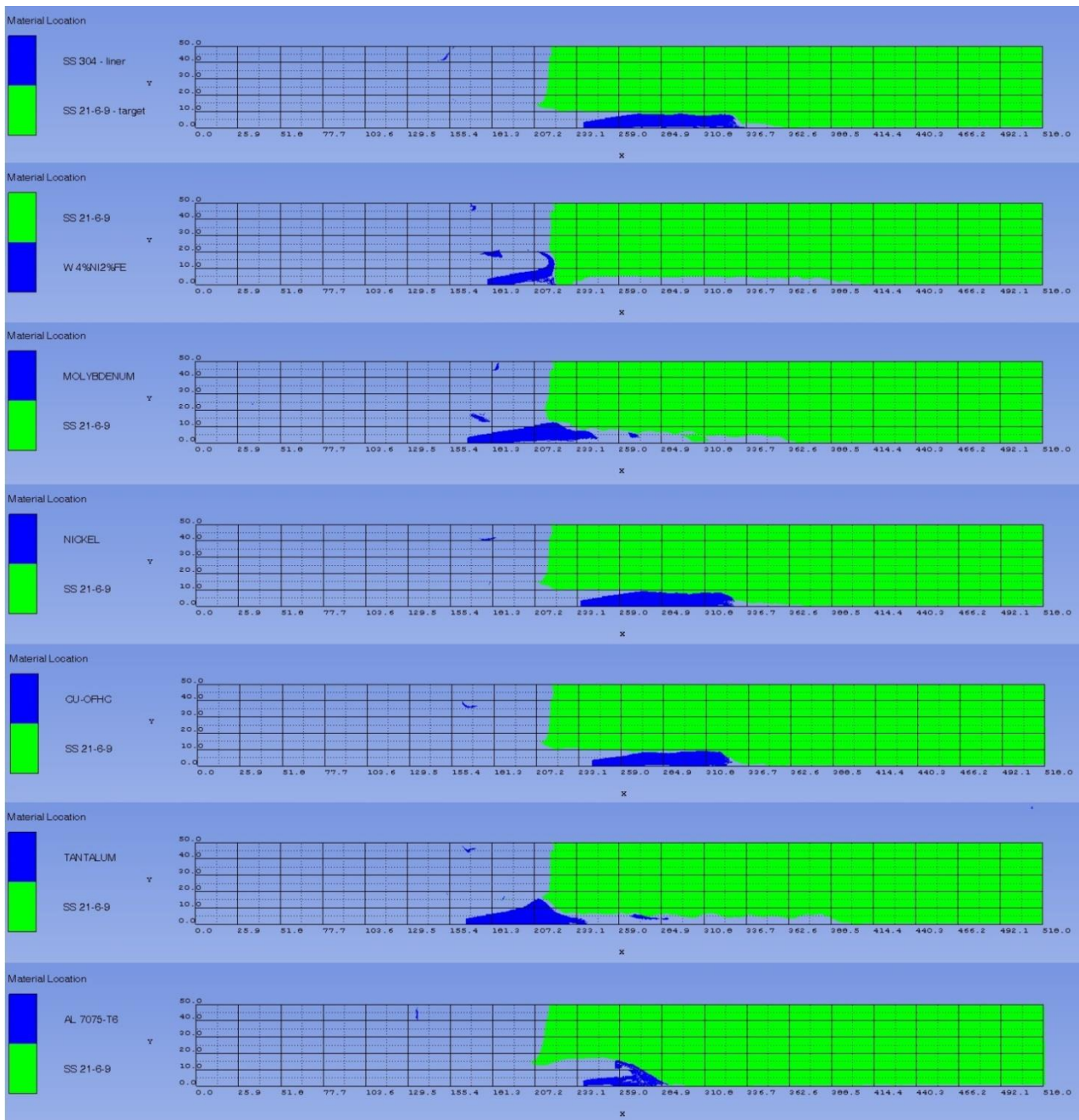

Figure 4.4.1 Penetration depths and holes made with liners of different materials (2D axisymmetric display); slugs can be seen at different position in the holes depending on the density of material

In summary, the choice of shaped charge liner material is usually a compromise between its mechanical properties (density, ductility, bulk-sound velocity, strength, melting temperature), ease of fabrication, and total costs. It is important to choose the most ductile material, with a density that is both high for greater penetration and low for a high jet tip velocity for a given amount of explosive, keeping other parameters as high as possible (bulk-sound velocity, strength, melting temperature).

Practical considerations, however, restrict the use of very expensive (for example gold, platinum) or toxic materials (for example depleted uranium - chemical toxicity is usually the major hazard from soluble forms of uranium, while the radiological hazard dominates inhalation of sparingly soluble forms [61]; lead - neurotoxin; some tungsten alloys are carcinogenic). The penetrating properties of other, more available materials, such as silver, molybdenum, tantalum, nickel for liners are also superior to that of conventional copper liner or steel liner, but this comes with the price - higher initial material costs, and in most cases also increased manufacturing and production costs.
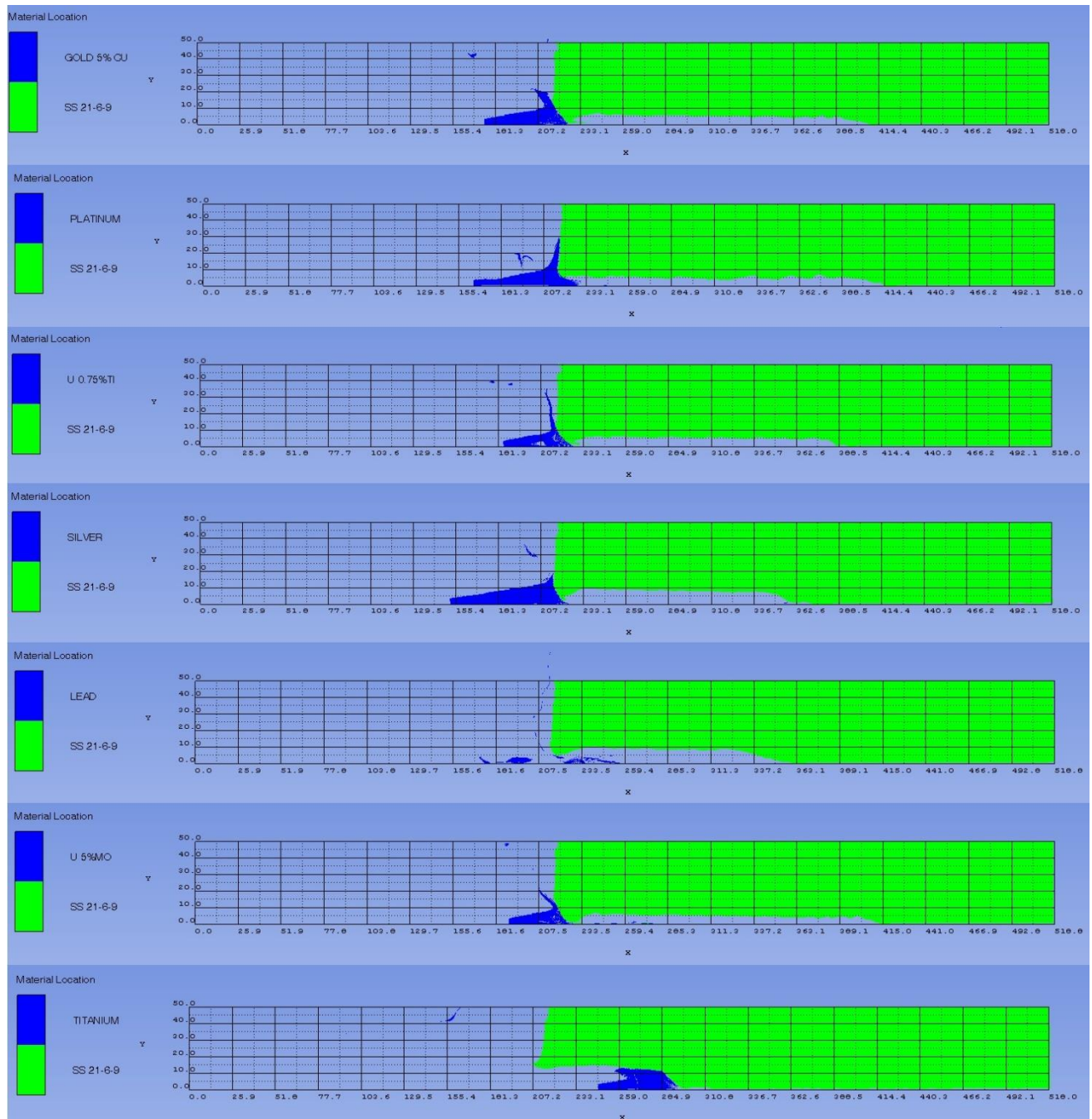

Figure 4.4.2 Penetration depths and holes made with liners of different materials; slugs can be seen at different position in the holes depending on the density of material

5. Conclusions

To ascertain the impact of various liner materials on the penetration depth into a steel target, numerical simulations of the Panzerfaust 30 (klein) anti-tank warhead were carried out using the Ansys AUTODYN program. It has been demonstrated that the selection of liner material can have a substantial impact on anti-tank ammunition's performance.

Materials such as platinum, gold, tantalum, tungsten, and depleted uranium alloys offer a substantial increase in penetration (up to 40%), albeit with significantly higher costs than using cheaper materials (copper, steel, lead), and with some of them being toxic or carcinogenic. Other, more available materials, such as silver, molybdenum, and nickel liners can potentially be superior to that of conventional copper or steel liners in terms of penetrating power but come also with higher total costs.

When larger entry holes, as well as pyrophoric and enhanced blast effect are needed, aluminum can potentially be the material of choice (high impact velocity). This, however, comes with a price - significantly reduced penetration depth. Titanium also showed a marked increase in the target hole diameter because of its higher impact velocity.

Further research can be an overall design optimization process for shaped charges warhead, involving many different parameters (for example warhead geometry up-scaling, optimizing the shape, thickness, and angle of the liner's tip, using more powerful explosives, optimizing casing thickness and stand-off distance, use of appropriate deviator, etc.) with optimal liner material, using numerical simulations and analytical methods, together with experimental data.

Declaration of competing interest

Funding information

References

[1] W. P. Walters, J. A. Zukas, Fundamentals and Theory of Shaped Charges, John Wiley & Sons, New York, 1989.

[2] J. Zukas, High velocity impact dynamics, Wiley Interscience, 1990.

[3] J. Carleone, Tactical Missile Warheads, Progress in Astronautics and Aeronautics, Volume 155, AIAA, 1993.

[4] J. A. Zukas, Introduction to Hydrocodes, Elsevier, 2004.

[5] E. Gurel, Modeling and Simulation of Shaped Charge, Doctoral thesis, Middle East Technical University, 2009.

[6] D. Fišerová, Numerical analyses of buried mine explosions with emphasis on effect of soil properties on loading, Doctoral thesis, Cranfield University, Defence College of Management and Technology, 2006.

[7] C. Poole, Penetration of Shaped Charge, Doctoral thesis, Corpus Christi College, University of Oxford, 2005.

[8] M. Held, "Liners for shaped charges", *Journal of Battlefield Technology*, Vol 4, No 3, November 2001.

[9] C. Wang, J. Ding. H. Zhao, "Numerical simulation on jet formation of shaped charge with different liner materials", *Defence Science Journal*, Vol. 65, No 4, pp. 279-286, 2015.

[10] T. A. E. Elshenawy, Criteria of design improvement of shaped charges used as oil well perforators, Doctoral thesis, University of Manchester, 2012.

[11] W. Kulsirikasem, A. Julniphitwong, G. Tanapornraweekit, "Investigation of materials for liners of shaped charge warhead and their optimum standoff distances", *The Second TSME International Conference on Mechanical Engineering*, Krabi, 19-21 October, 2011.

[12] S. Buc, Shaped Charge Liner Materials: resources, processes, properties, costs and applications, Advanced Research Projects Agency (ARPA), Technical report, SPC 91-282-2, 1991.

[13] G. R. Johnson, W. H. Cook, "A constitutive model and data for metals subjected to large strains, high strain rates and high temperatures", *Proceedings 7th International Symposium on Ballistics*, pp. 541-547, The Hague, 1983.

[14] W. Walters, Introduction to shaped charges, ARL-SR-150, March, 2007.

[15] L. Ding, W. Tang, X. Ran, "Simulation study on jet formability and damage characteristics of a low-density material liner", *Materials*, January, 2018.

[16] W. T. Fu, Z. H. Rong, "Copper-tungsten shaped charge liner and its jet", *Propellants, Explosives, Pyrotechnics*, Vol. 21, No. 4, pp. 193-195, 1996.

[17] B. Bourne, K. G. Cowan, J. P. Curtis, "Shaped charge warheads containing low melt energy metal liners", *19th International Ballistic Symposium*, Interlaken, Switzerland, May 7-11, 2001.

[18] W. Tie-Fu, Z. He-Rong, "Copper-Tungsten Shaped Charge Liner and its Jet", *Propellants, Explosives, Pyrotechnics*, Vol. 21, pp. 193- 196, 1996.

[19] Z. Zhao, J. Liu, W. Guo, S. Li, G. Wang, "Effect of Zn and Ni added in W–Cu alloy on penetration performance and penetration mechanism of shaped charge liner", *International Journal of Refractory Metals and Hard Materials*, Vol. 54, pp. 90-97, 2016.

[20] S. V. Fedorov, A. V. Babkin, S. V. Ladov, G. A. Shvetsov, A. D. Matrosov, "On the possibility of reducing the penetration capability of shaped-charge jets in a magnetic field", *Journal of Applied Mechanics and Technical Physics*, Vol. 48, No. 3, pp. 393-400, 2007.

[21] W. Q. Guo, J. X. Liu, Y. Xiao, S. K. Li, Z. Y. Zhao, J. Cao, "Comparison of penetration performance and penetration mechanism of W-Cu shaped charge liner against three kinds of target: pure copper, carbon steel and Ti-6Al-4V alloy", *International Journal of Refractory Metals & Hard Materials*, Vol. 60, pp. 147-153, 2016.

[22] N. D. Gerami, G. H. Liaghat, G. H. R. S. Moghadas, N. Khazraiyan, "Analysis of liner effect on shaped charge penetration into thick concrete targets", *Journal of the Brazilian Society of Mechanical Sciences and Engineering*, Vol. 39, No. 8, pp. 3189-3201, 2017.

[23] K. Naeem, A. Hussain, S. Abbas, "A Review of Shaped Charge variables for its optimum performance", *Engineering, Technology & Applied Science Research*, Vol. 9, No. 6, pp. 4917-4924, 2019.

[24] J. Xiao, X. Zhang, Z. Guo, H. Wang, "Enhanced damage effects of multi-layered concrete target produced by reactive materials liner", *Propellants, Explosives, Pyrotechnics*, Vol. 43, No. 9, pp. 851-851, 2018.

[25] B. Zygmunt, Z. Wilk, "The research of shaped charges with powder liners for geological borehole perforation", *Archives of Mining Sciences*, Vol. 52, No. 1, pp. 121-133, 2007.

[26] W. Walters, P. Peregino, R. Summers, D. Leidel, "A study of jets from unsintered-powder metal lined nonprecision small-caliber shaped charges", *USA Army Ballistics Research Laboratory*, Aberdeen Proving Ground, 2001.

[27] B. Grove, "Theoretical considerations on the penetration of powdered metal jets", *International Journal of Impact Engineering*, Vol. 33, No. 1-12, pp. 316-325, 2006.

[28] N. Duan, Y. Gao, J. Wang, W. Du, F. Wang, "The properties of the sintered copper powder liner", *Journal of Wuhan University of Technology - Materials Science Edition*, Vol. 29, No. 2, pp. 269-272, 2014.

[29] Y. Wang, Q. Yu, Y. Zheng, H. Wang, "Formation and penetration of jets by shaped charges with reactive material liners", *Propellants, Explosives, Pyrotechnics*, Vol. 41, No. 4, pp. 618-622, 2016.

[30] T. Majewski, A. Jackowski, "Use of graphene for shaped charge liner materials", *Problems of Mechatronics Armament, Aviation, Safety Engineering*, Vol. 9, No 3, pp. 15-28, 2018.

[31] N. Santosh et al, "Improvement in performance of shaped charge using bimetallic liner", *Explosion Shock Waves and High Strain Rate Phenomena*, Materials Research Proceedings 13, pp. 141-148, 2019.

[32] AUTODYN® - Explicit Software for Nonlinear Dynamics, Theory Manual - Revision 4.3, Century Dynamics Inc., 2005.

[33] Ansys Autodyn Training Manual: Euler Solver, ANSYS Inc., 2009.

[34] J. Tu, G. H. Yeoh, Ch. Liu, Computational Fluid Dynamics - A Practical Approach, Third Edition, Elsevier Ltd, 2018.

[35] A. Elbeih, T. Elshenawy, S. Zeman, Z. Akstein, "Application of BCHMX in shaped charges against RHA targets compared to different nitramine explosives", *Central European Journal of Energetic Materials*, Vol 15, No 1, pp. 3-17, 2018.

[36] T. Elshenawy, A. Elbeih, Q. M. Li, "Influence of target strength on the penetration depth of shaped charge jets into RHA targets", *International Journal of Mechanical Sciences*, Volume 136, pp. 234-242, February 2018.

[37] E. E. El-Sayed, T. A. Elshenawy, M. A. Shaker, A. M. Riad, "Influence of different shaped charge parameters on jet penetration into metallic target", *Journal of Physics: Conference Series 2299 012016*, IOP Publishing, 2022.

[38] T. J. Gander, Field Rocket Equipment of the German Army 1939-1945, Almark Publishing, 1972.

[39] S. J. Zaloga, Panzerfaust vs Sherman - European Theater 1944-45, Osprey Publishing, 2019.

[40] G. L. Rottman, Panzerfaust and Panzerschreck, Osprey Publishing, 2014.

[41] S. V. Ivanov, Soldier on front No 60: Panzerfaust and Panzerschreck, ARS, 2010.

[42] German explosive ordnance - projectiles and projectile fuzes, TM 9-1985-3, United States Government Printing Office, Washington, 1953.

[43] W. Fleischer, Panzerfaust and other German infantry anti-tank weapons, Schifer Publishing, 1994.

[44] C. Bishop, The Encyclopedia: Weapons of World war II, Barnes & Noble, 1998.

[45] J. A. Zukas, Introduction to Hydrocodes, Elsevier, 2004.

[46] B. M. Dobratz, P. C. Crawford, LLNL Explosives Handbook - Properties of Chemical Explosives and Explosive Simulants, January 31, 1985.

[47] J. Carleone, Tactical Missile Warheads, Progress in Astronautics and Aeronautics, Volume 155, AIAA, 1993.

[48] D. J. Steinberg, S. G. Cochran, M. W. Guinan, "A constitutive model for metals applicable at high-strain rate", *J. Appl. Phys.*, Vol 51, No 3, March 1980.

[49] G. E. Fairlie, "The Numerical Simulation of High Explosives using AUTODYN-2D & 3D", *Explo '98, Institute of Explosive Engineers 4th Biannual Symposium*, September 1998.

[50] H. Seidler, Hitler's Anti-Tank Weapons 1939–1945 (Images of War), Pen and Sword Military, May 13, 2020.

[51] https://www.techsteel.net/alloy/stainless-steel/21-6-9

[52] https://www.thyssenkrupp-materials.co.uk/stainless-steel-304-14301.html

[53] R. DiPersio, W. Jones, A. Merendino, J. Simon, Characteristics of jets from small caliber shaped charges with copper and aluminum liners, BRL Technical Report No. 1866, September, 1967.

[54] H. O. Agu, The effect of 3D printed material properties on shaped charge liner performance, Dissertation thesis, Cranfield University, Defence and Security, 2019.

[55] B. Bourne, K. G. Cowan, J. P. Curtis, "Shaped charge warheads containing low melt energy metal liners", *19th International symposium on Ballistics*, 2001.

[56] B. Zygmunt, Z. Wilk, "Formation of jets by shaped charges with metal powder liners", *Propellants, Explosive, Pyrotechnics*, Vol 33, No 6, pp. 482-487, 2008.

[57] https://www.metal.com/

[58] https://pubs.usgs.gov/periodicals/mcs2022/mcs2022-tantalum.pdf

[59] https://tradingeconomics.com/commodity/molybden

[60] https://web.evs.anl.gov/uranium/guide/ucompound/propertiesu/brochure.cfm

[61] Depleted Uranium - Technical brief, United States Environmental Protection Agency, Office of Air and Radiation Washington, EPA-402-R-06-011, December 2006.

[62] R. Xu, Li Chen, Jinhua Zhang, Hengbo Xiang, Qin Fang, "Penetration of an optimal depleted uranium liner of a shaped charge: A numerical simulation method", *International Journal of Protective Structures*, Volume 12, No 3, 2021.

[63] B. E. Fuchs, Shaped charges having a porous tungsten liner-an experimental and theoretical study of metal compression, jet formation and penetration mechanics, Dissertation thesis, New Jersey Institute of Technology, 1997.

[64] Selected Hugoniots, Prepared by Group GMX-6, Los Alamos Scientific Laboratory, University of California, May 1, 1969.